EVALUATION OF THE EFFECTS OF PHYSICAL AND CHEMICAL HETEROGENEITIES ON FLOW AND TRANSPORT IN THE SATURATED ALLUVIUM OF FORTYMILE WASH, NEVADA

Prepared for

U.S. Nuclear Regulatory Commission
Contract NRC–02–02–012

Prepared by

Alexander Y. Sun
F. Paul Bertetti

Center for Nuclear Waste Regulatory Analyses
San Antonio, Texas

October 2007

ABSTRACT

The saturated alluvium of Fortymile Wash is conceptualized as a natural barrier to the transport of radionuclides that might be released from the potential high-level waste repository at Yucca Mountain. Previous analyses conducted by the Center for Nuclear Waste Regulatory Analyses (CNWRA) using borehole cutting logs and outcrop studies indicated that the saturated alluvium of Fortymile Wash, Nevada, consists of highly permeable hydrofacies that are embedded in less permeable hydrofacies at a multiplicity of scales. The more permeable facies, if well connected, can form preferential fast flow paths for radionuclide transport. The physical heterogeneity is also a factor leading to spatial variability in sorption parameters. Because of computational limitations, the current process-level, site-scale saturated zone flow and transport models are represented and solved on coarse numerical grids, resulting in a loss of subgrid information. Neither the physical nor the chemical heterogeneity in the alluvium is explicitly accounted for in site-scale saturated zone models. Transport in the saturated alluvium is modeled by solving the classical advection dispersion equation with identical dispersivities assigned to each grid block. The site-specific information on subgrid physical and chemical heterogeneities, which are known to affect grid block scale flow and transport in highly heterogenous aquifers, was not used explicitly in determining the equivalent flow and transport properties. A number of field and laboratory experiments have been carried out since these site-scale models were created. Understanding of the flow and transport uncertainties at the block scale can thus be strengthened by using the new information from the field and laboratory experiments.

This report summarizes numerical experiments conducted at the CNWRA to quantify the effects of subgrid physical and chemical heterogeneities. Monte Carlo simulations are performed using realizations of a fine-scale block model for which the properties are generated stochastically based on a hierarchical alluvium facies model. The statistics of Neptunium sorption parameters are derived from data pertaining to the Fortymile Wash alluvial aquifer. Transport is solved in a Lagrangian framework in which the solute mass is divided into a large number of particles, which are then displaced using an efficient random walk algorithm. The results indicate that the upscaled block hydraulic conductivities have similar magnitudes as those assigned to the alluvium in site-scale models. The simulated longitudinal macrodispersivities are on the order of 10 m [32.8 ft], depending on the variance of hydraulic conductivities. The results of reactive transport modeling show that retardation introduces at most a two-fold increase in solute spread in the longitudinal direction. In the basecase, no correlation in K_A is assumed. Additional sensitivity studies show that correlation in K_A may reduce plume spread.

CONTENTS

FIGURES

TABLES

ACKNOWLEDGMENTS

This report was prepared to document work performed by the Center for Nuclear Waste Regulatory Analyses (CNWRA) and its contractors for the U.S. Nuclear Regulatory Commission (NRC) under Contract No. NRC–02–02–012. The activities reported here were performed on behalf of the NRC Office of Nuclear Material Safety and Safeguards, Division of High-Level Waste Repository Safety. This report is an independent product of CNWRA and does not necessarily reflect the views or regulatory position of NRC.

The authors wish to thank S. Painter for technical review, L. Mulverhill for editorial review, G. Wittmeyer for programmatic review, and finally, J. Simpson for her tireless administrative support.

QUALITY OF DATA, ANALYSES, AND CODE DEVELOPMENT

DATA: The original CNWRA-generated data contained in this report meet quality assurance requirements described in the CNWRA Quality Assurance Manual. Data used to compile this report may be found in CNWRA Scientific Notebooks 719E and 746E.

ANALYSES AND CODES: The analyses in this report are documented according to CNWRA quality assurance procedures in Scientific Notebooks 746E and 719E.

The Transition Probability Geostatistical Software Version 2.1 (T-ProGS) (Carle, 1999) was used to construct Markov chain models of facies spatial variability and generate realizations of facies distributions. Modules from the Geostatistical Software Library (Deutsch and Journel, 1998) were used to generate random fields for use in Monte Carlo simulations. MODFLOW-2000 (Harbaugh, et al., 2000) was used to solve for groundwater flow models. Mass transport simulation was performed using SLIM-FAST (Maxwell and Tompson, 2006). All inputs and outputs for analyses contained herein are documented in CNWRA Scientific Notebook 746E.

REFERENCES:

Carle, S.F. "T-PROGS: Transition Probability Geostatistical Software, Version 2.1." Davis, California: University of California. 1999.

Deutsch, C.V. and A.G. Journel. "Geostatistical Software Library and Users Guide." Second Edition. New York City, New York: Oxford University Press. 1998.

Harbaugh, A.W., E.R. Banta, M.C. Hill, and M.G. McDonald. "MODFLOW-2000, the U.S. Geological Survey Modular Ground-Water Model-User Guide to Modularization Concepts and the Ground-Water Flow Process." U.S. Geological Survey Open-File Report 00-92. 2000.

Maxwell, R.M. and A.F.B. Tompson. "SLIM-FAST: A User's Manual." UCRL–SM–225092. Livermore, California: Lawrence Livermore National Laboratory. 2006.

1 INTRODUCTION

1.1 Background

Yucca Mountain, Nevada, is the site for a potential geologic repository for permanent disposal of high-level nuclear waste. A critical performance requirement for such a nuclear waste repository is that it must include both natural and engineered barriers. Although the saturated zone below Yucca Mountain constitutes a potential pathway for radionuclides to reach the accessible environment, the porous media in the saturated zone is also expected to act as a natural barrier to radionuclide transport. In particular, the alluvial aquifer of Fortymile Wash, located just upstream of the 18-km [11.2-mi] compliance boundary, is conceptualized as the most significant component of the saturated zone natural barrier mechanism because of the slower groundwater flow velocity (compared to that of the upstream volcanic tuff aquifers) and higher sorption capacity associated with the saturated alluvium. Both DOE and the U.S. Nuclear Regulatory Commission (NRC) identified the retardation of radionuclides in the saturated alluvium of Fortymile Wash as a process that is important to isolating high-level waste (Bechtel SAIC Company, LLC, 2004; NRC, 2004).

Retardation in the saturated alluvium primarily occurs through sorption, which includes such processes as adsorption, surface precipitation, and absorption. In performance assessment abstraction models, sorption is often represented using a linear equilibrium sorption model, which is specified mainly through an empirically derived distribution coefficient, K_d. The linear equilibrium sorption model inherently assumes that the sorption process is reversible, has no maximum value for sorption and site saturation, and is independent of variations in water chemistry and mineralogy. Experimental and theoretical studies, however, show that the sorption behavior can deviate significantly from the linear equilibrium model. To compensate some of the limitations of the simple linear equilibrium model, a typical approach in performance assessment is sampling values from a range of values that are representative of sorption under expected variations in conditions (Bertetti, et al., 2004). Variations in sorption capacity in the saturated alluvium are driven not only by the particular solid phases that are present, but also by geochemistry. For example, experiments show that the sorption coefficients of actinides (Am, Np, Pu, Th, U) are sensitive to pH and to the concentration of carbonate species in groundwater (Bertetti, et al., 1998; Davis, 2001).

In current DOE and NRC performance assessment codes, spatial variability in K_d is handled by assigning different K_d values to different types of hydrostratigraphic units found at Yucca Mountain (Bertetti, et al., 2004). Physical and chemical heterogeneities exist within each hydrostratigraphic unit. In the alluvium, physical heterogeneity is mainly manifested as the interbedding of different hydrofacies potentially creating compartmentalized flow and transport regimes in the system. Modeling variations of sorption at the field scale can be a an uncertain process, even with the simple linear equilibrium sorption model. This is not only because the relevant data are scarce and are usually obtained at smaller scales (e.g., laboratory scale), but also because the effects of the physical and chemical heterogeneities are coupled: variations of the minerals comprising solid phases of a system can strongly affect the groundwater chemistry and the geochemical processes involved; similarly, mineral precipitation and dissolution processes can also alter the hydrodynamic behavior of the system.

The current site-scale saturated zone flow and transport models are discretized into coarse numerical blocks that span hundreds of meters horizontally and tens of meters vertically

(Bechtel SAIC Company, LLC, 2004; Winterle, 2003; Farrell, et al., 2005). Equivalent flow and transport parameters, obtained through either model calibration or expert elicitation, are assigned to the numerical blocks. Many of the tracer field experiments documented in the literature were conducted in sites (e.g., the Borden site and Cape Cod site) with relatively mild heterogeneities. Thus, observations and opinions based on those experiments may not be directly applicable to predicting solute transport in highly heterogeneous aquifers having log-conductivity variances greater than 1. Rehfeldt, et al. (2004) suggested that if significant flow variability is ignored, the dispersivity will be overestimated. Predictions made with the larger dispersivity in a uniform flow field will overestimate dilution and, thus, give rise to lower dose estimation.

When deriving equivalent parameters for use in coarse block models, a fundamental assumption is that the equivalent parameters are capable of representing the underlying physical and chemical heterogeneities. Recent studies suggest that the equivalent parameters may not be fully representative of the subgrid variability and can be sensitive to changes in flow and transport conditions (e.g., Farmer, 2002; Rubin, 2003; de Marsily, et al., 2005). The mixing of a plume about its centroid and the motion of the plume's centroid are largely defined by different scales of variability (Rubin, 2003). A coarse resolution numerical model may capture the large-scale variability, but the effects of mixing caused by subgrid variability are lost. An important concern is whether or not parameters used in the current site-scale models and abstraction models adequately capture the large-scale effect originated from subgrid variability.

The main goals of this study are to

- Understand flow and transport in the heterogeneous alluvium using a previously developed alluvium facies model
- Quantify the effects of subgrid physical and chemical heterogeneities on radionuclide transport via Monte Carlo simulation
- Assess the variability of the upscaled block hydraulic conductivity
- Assess the variability of the block dispersivity values

The outcome of this study complements the previous CNWRA sedimentological modeling efforts (Ressler, et al., 2000; Sun, et al., 2006; Sun, et al.[1] and geochemistry laboratory analyses (Bertetti, et al., 2004).

1.2 Literature Review

The effects of physical and chemical heterogeneity on field-scale transport processes have been subject to extensive studies in the past (e.g., Dagan, 1989; Gelhar, 1993; Naff, et al., 1998; Attinger, et al., 1999; Ginn, 2001; Cortis, et al., 2004; Berkowitz, et al., 2006, 2002).

[1]Sun, A.Y., R. Ritzi, and D. Sims. "Characterization and Modeling of Spatial Variability in a Complex Alluvial Aquifer: Implications on Solute Transport." *Water Resources Research*. 2007. (Submitted for publication).

It has been demonstrated experimentally and numerically that small-scale heterogeneities can contribute significantly to the observed large-scale transport behavior (e.g., Gelhar, et al., 1992; Brusseau, 1994; Harvey and Gorelick, 2000; Cirpka, 2002; Liedl and Ptak, 2003; Fernàndez-Garcia and Gómez-Hernández, 2007). Despite the previous efforts, the question of how to best integrate resolved and unresolved heterogeneities remains an open problem. A main source of uncertainty stems from the fact that the scale of interest for model outcomes is rarely the scale for which information is available. For example, the scale of K_d measurements is usually less than a meter [1 m = 3.28 ft]. In comparison, the dimensions of numerical blocks in site-scale saturated zone models are usually on the order of hundreds of meters horizontally and tens of meters vertically.

A key issue is how to appropriately represent unresolved variability as well as the local dispersion and mass transfer processes in field-scale models. Upscaling generally refers to the process of extrapolating system characteristics at the scale of direct observation to the numerical block scale. Approaches for upscaling parameters of the single-phase flow equation (e.g., porosity and hydraulic conductivity) can be classified into simple power averaging schemes and flow-based methods. The latter approaches involve solving the flow equations explicitly on a fine grid to obtain the effective parameters for use on a coarser grid (cf., de Marsily, et al., 2005; Durflosky, 2005).

Upscaling transport parameters is more complicated, especially for reactive transport. When applying the classical advection dispersion equation at the field scale, a common assumption is that the dispersivity tensor can be enhanced to account for the loss of small-scale information. The macrodispersion theory (cf., Dagan, 1989; Gelhar, 1993) attempts to explain the scale dependency of the transport phenomena by replacing the dispersion tensor in the classical advection–dispersion equation with a macrodispersion tensor. Rubin, et al. (1999) introduced the concept of block dispersivity to compensate for the loss of subgrid heterogeneity resulting from flow parameter upscaling. Fernàndez-Garcia and Gómez-Hernández (2007) recently validated the performance of block dispersivity theory numerically and observed that the upscaled transport models can largely underestimate the spreading of solute plumes, even if block dispersivities are calculated as representative of within-block heterogeneity. They also pointed out the need for considering off-diagonal components of the upscaled hydraulic conductivity tensor in transport modeling. The continuous time random walk approach (Berkowitz, et al., 2006, 2002; Cortis, et al., 2004) has been proposed as a unified framework for taking account of different levels of uncertainty associated with characterizing heterogeneities at different spatial scales.

After reviewing a large number of studies on field-scale dispersion, Rehfeldt, et al. (2004) made a number of conclusions, of which a few are listed here:

- Longitudinal dispersion is scale dependent. Dispersivities measured with tracer test-scale experiments (up to a few hundred meters) are almost certainly not applicable to large-scale simulations on the scale of thousands to tens of thousands of meters.

- Transverse dispersion is an important parameter. Several studies contend that true dilution of a plume comes from the small transverse dispersion terms that become important as the plume gets large.

- Stationary random field assumptions, self-similar fields with low wave number cutoffs, or plume-scale averaging all lead to situations where the longitudinal dispersivity reaches an asymptotic value.

- Self-similar random fields or strongly heterogeneous fields that exhibit channeling or other "nonergodic" behavior tend to lead to dispersion coefficients that grow large at large distances.

In the following sections, previous analyses pertaining to the goals of this study are summarized.

1.3 Previous Studies

The DOE saturated zone radionuclide transport abstraction model assigns the same longitudinal dispersivities to the tuff and alluvium units. The assigned longitudinal dispersivities were sampled from a truncated lognormal distribution with a mean of 2.0 and a standard deviation of 0.75. This corresponds to a mean longitudinal dispersivity of 100 m [328 ft] with an upper 95-percent confidence limit of 3.2 km [2 mi]. The sampled longitudinal dispersivity values were further scaled down by a factor of 10 when represented on the scale of 500 m [1,640 ft], the horizontal dimension of computational grid blocks in the DOE site-scale saturated zone transport model. Thus, the longitudinal dispersivity value used in the DOE basecase saturated zone transport model is 10 m [32.8 ft]. The transverse and vertical dispersivities were obtained by dividing the longitudinal dispersivity by 200 and 20,000, respectively (Bechtel SAIC Company, LLC, 2004). All DOE site-scale saturated zone flow and transport models are under revision at the time of this writing (Al-Aziz, et al., 2006).

In response to a recommendation from an expert panel (Geomatrix Consultants, 1998) to study the amount of dispersion that could occur within a single gridblock of the site-scale transport model, McKenna, et al. (2003) used high-resolution stochastic continuum models to estimate the transverse and longitudinal macrodispersion that may occur at the subgrid scale within the DOE saturated zone site-scale model. The dimensions of the block model used in McKenna, et al. (2003) were defined as 496 × 496 × 48 m [1627 × 1627 × 157 ft]. The enhanced permeability fields were generated by superimposing a network of high-permeability features onto a background permeability model, which was generated based on data derived from the volcanic tuff aquifers at Yucca Mountain. McKenna, et al. (2003) observed that longitudinal macrodispersivities calculated with the enhanced permeability model reached a value of 2,380 m [7,808 ft] after 460 m [1,509 ft] of travel and appeared to still be rising. The results of McKenna, et al. (2003), however, were not used directly to support the transport abstraction model. The purpose of the current study is similar to that of McKenna, et al. (2003), except that the focus will be on flow and transport in the alluvium rather than the fractured tuff aquifer.

Sun, et al.[2] developed a hierarchical hydrofacies model for the alluvial aquifer of Fortymile Wash. The model is based on multiple data sources, such as borehole cutting logs collected from Nye County Early Warning Drilling Program (Nye County Nuclear Waste Repository Project Office, 2007), the Fortymile Wash outcrop study conducted by Ressler, et al. (2000), and empirical scaling relationships derived from studying the dimensions of fluvial bedforms as

[2]Ibid.

a function of channel width (Lunt, et al., 2004). The major outcome from the Sun et al.[3] investigation is a three-dimensional Markov chain model of facies transition probabilities, which can be used to generate geologically plausible realizations of facies distributions in the Fortymile Wash alluvial aquifer. The alluvium facies model, after appropriate upscaling, can be linked to the existing site-scale saturated zone flow model to represent site-scale flow and transport or can be used to assess the effect of subgrid heterogeneity on upscaled flow and transport parameters. The latter is the main focus in the current study.

Painter, et al. (2001) conducted process-level analyses to quantify the effects of physical heterogeneity (hydraulic conductivity) and chemical heterogeneity (K_d) on radionuclide retardation in the alluvial aquifer near Yucca Mountain. The hydraulic conductivity, *K,* was modeled using a unimodal lognormal distribution with exponential spatial covariance function. The spatial variability of K_d for Np was modeled in a similar fashion, based on a saturated zone geochemistry data set collected from 238 sample locations in the vicinity of Yucca Mountain (Turner and Pabalan, 1999). Uncertainty associated with mass transport was quantified using a two-site, mobile–immobile mass transfer model formulated in the stochastic streamtube framework (Cvetkovic and Dagan, 1994), and an instantaneous point source was assumed. Painter, et al. (2001) conclude that the effect of physical heterogeneity is important; however, chemical heterogeneity and the correlation between *K* and K_d have minimal effect. They also found that treating K_d as a spatially constant but uncertain parameter greatly overemphasizes the effect of K_d variability and thus yields conservative estimates.

Analyses of radionuclide sorption data from Frenchman Flat alluvium in the Nevada Test Site indicated that spatial heterogeneity of radionuclide-sorbing materials can have a large impact on radionuclide transport (Tompson, et al., 1999; Carle, et al., 2002; Zavarin, et al., 2004). If uniform properties are used in the large-scale transport models, the radionuclide transport may not be accurately predicted.

A number of K_d samples pertaining to the alluvium in the Fortymile Wash region have been collected and analyzed by CNWRA staff since the Painter, et al. (2001) study. The new information warrants a fresh investigation of the effects of physical and chemical heterogeneities on radionuclide transport in the alluvial aquifer of Fortymile Wash.

[3]Ibid.

2 METHODOLOGY

2.1 Overview

A fine-scale, three-dimensional, block model is used in this study to evaluate the effects of subgrid heterogeneities. The general workflow consists of four main steps:

- First, a three-dimensional model having dimensions of a representative numerical block in the NRC site-scale model is created. The horizontal dimensions of the block model are 300 × 300 m [984.3 × 984.3 ft] and the vertical dimension is 20 m [65.6 ft].

- Second, the block model is discretized by a fine grid. The hierarchical alluvium hydrofacies model developed by Sun, et al.[1] is used to generate random facies distributions in the block model. The facies distributions are then related to hydraulic conductivity and sorption parameter distributions. An ensemble of such random distributions, constructed using the principle of stochastic simulation, is used to represent a range of spatial heterogeneities captured by the underlying facies model.

- Third, the uncertainties associated with the subgrid heterogeneity are quantified through Monte Carlo simulation in which the groundwater flow and transport questions are solved using the block model.

- Fourth, the upscaled block hydraulic conductivities, as well as the block macrodispersivities, are calculated.

Figure 2-1 illustrates the main steps in this workflow. The details of each step are described below.

2.2 The Hierarchical Alluvium Model

The hierarchical hydrofacies model of the Fortymile Wash alluvial aquifer (Sun, et al.[2]) consists of two levels, which are classified corresponding to the scales of bedforms and deposits and to the contrasts in permeabilities. Level I of the hierarchy refers to smaller scale hydrofacies and Level II larger scale hydrofacies.

At Level II, the higher permeability hydrofacies are braid-belt deposits and the lower permeability hydrofacies are paleosols. A braid-belt deposit includes mostly compound-bar deposits with minor occurrences of circumscribed channel fills. The compound-bar deposits have two scales of internal cross stratification created by unit bars and dunes. The pedogenic processes forming paleosols operated on the tops of compound bars because they were subareally exposed for significant periods of time. The regions inside paleosols are not further delineated.

---

[1]Sun, A.Y., R. Ritzi, and D. Sims. "Characterization and Modeling of Spatial Variability in a Complex Alluvial Aquifer: Implications on Solute Transport." *Water Resources Research*. 2007. Submitted for publication.

[2]Ibid.

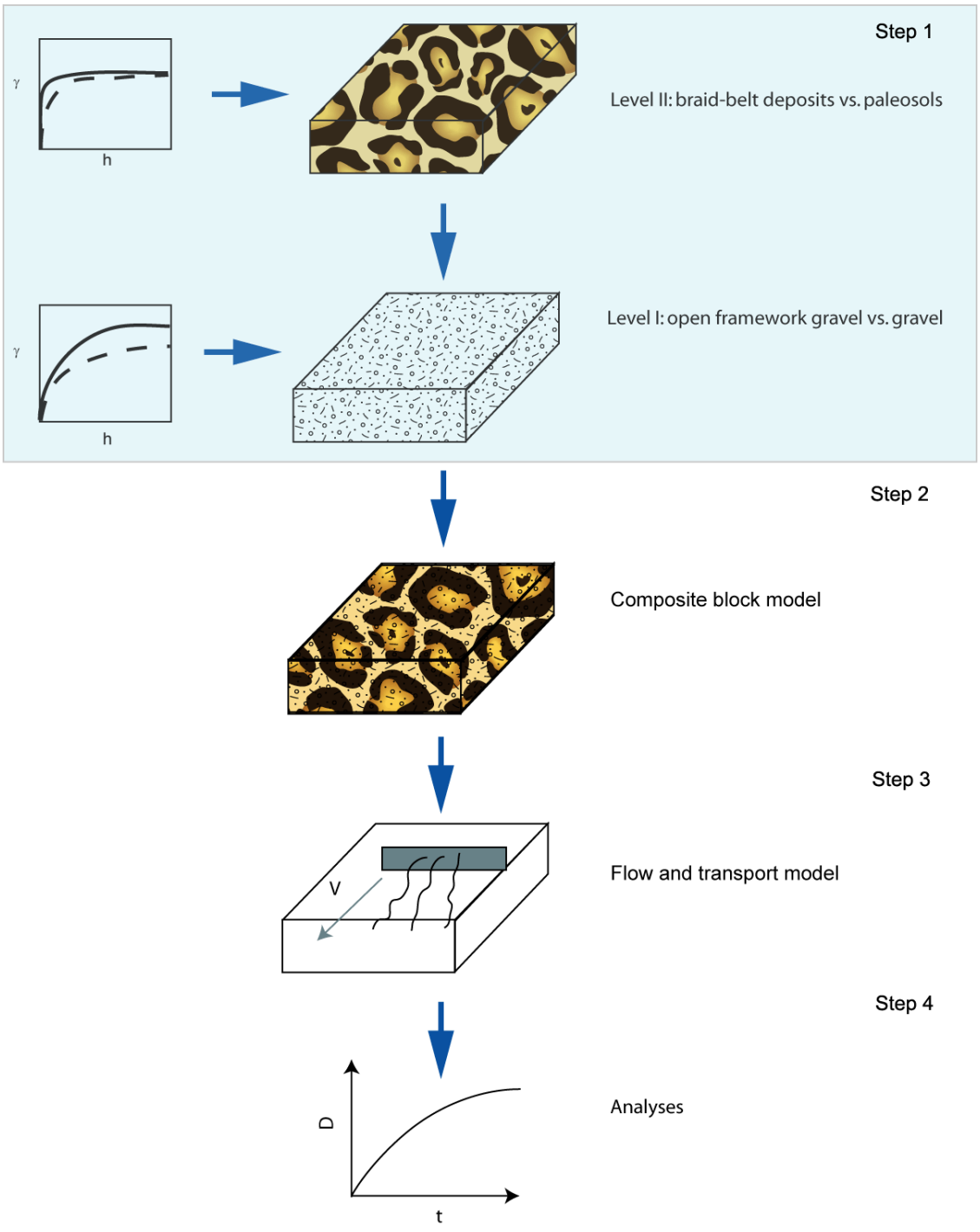

Figure 2-1. Flow Diagram Illustrating the Main Steps Followed in This Investigation. The Highlighted Area Illustrates the Generation of Composite Hydraulic Conductivity Fields. The Effects of Fine-Scale Heterogeneities on Block-Scale Flow and Transport Are Investigated Via Monte Carlo Simulation.

At Level I, regions inside the higher permeability, braid-belt bars are further delineated according to the larger permeability contrasts. The higher permeability hydrofacies of Level I are the open framework gravel strata created by dune bedforms, and the lower permeabilty hydrofacies are nonopen framework gravel regions.

Statistics of each of the hydrofacies are summarized in Table 2-1 (adapted from Table 1 of Sun, et al.[3] where data pertaining to the Fortymile Wash alluvial aquifer were used. Table 2-1 shows that there are nearly two orders of magnitudes of contrast in mean hydraulic conductivity between the most permeable facies and the least permeable facies. The differences in mean lengths, which is an indicator of the spatial continuity of facies, is substantial. The hierarchical model reflects the multiscale nature of the natural formations observed in many field investigations.

2.3 Upscaling of Hydraulic Conductivity

Upscaling of flow equation parameters is routinely performed in petroleum reservoir simulation and groundwater modeling to alleviate the computational burden associated with solving the fine-resolution model. For single-phase flow involving a single component, only hydraulic conductivity and porosity need to be upscaled. The common upscaling approaches are power-averaging schemes and flow-based approaches. Power-averaging schemes are the simplest methods for upscaling (Durflosky, 2005)

Table 2-1. The Statistics of the Hydrofacies of the Hierarchical Alluvium Model

Level	Direction	Unit Type	Volume Proportion	Mean Length (m*)	ln*K* Correlation Length (m)	Mean ln*K*
II	Vertical	Paleosol	0.2	3.5	2	-1.609
		Braid-belt	0.8	14	2	1.386
	Horizontal	Paleosol	0.2	1,400	10	-1.609
		Braid-belt	0.8	5,600	10	1.386
I	Vertical	OFG†	0.2	2	2	2.51
		Non-OFG	0.8	8	2	0.21
	Horizontal	OFG	0.2	10	10	2.51
		Non-OFG	0.8	40	10	0.21

*1 m = 3.28 ft
†OFG = Open framework gravel

[3]Ibid

$$K_i^* = \left(\frac{1}{V_b} \int_{V_b} [K_i(\mathbf{x})]^{\omega_i} dV \right)^{1/\omega_i} \quad (2\text{-}1)$$

where $K_i(\mathbf{x})$ is the fine-scale hydraulic conductivity tensor, *and* K_i^* is the upscaled hydraulic conductivity tensor, both of which are considered diagonal tensors; V_b is the averaging volume, and the power exponent ω_i is constrained to lie between −1 and 1 and can vary with direction *i*. For perfectly layered formations, ω is equal to 1 for flow parallel to the layers (arithmetic) and −1 for flow perpendicular to the layers (harmonic).

Flow-based methods more robustly and accurately compute upscaled hydraulic conductivity tensors. The effective block hydraulic conductivities in this report are calculated by solving the groundwater flow equation over the fine grid, where the boundaries of the domain are subject to constant head and no-flow boundary conditions. Figure 2-2 illustrates the problem configuration of flow-based upscaling for a two-dimensional problem. For example, the effective hydraulic conductivity along x_1 is found by imposing constant-head boundaries along the x_1 direction and no-flow boundaries along the x_2 direction. The effective hydraulic conductivity can then be computed by dividing the total flux from the fine-scale solution by the flow rate that would be found for a homogeneous region of upscaled hydraulic conductivity K_1^*, or

$$K_1^* = \frac{q_1}{(\Delta h / L_1) L_2 L_3} \quad (2\text{-}2)$$

where L_i, i = 1,2,3, are the block dimensions, q_1 is the total flux from the fine-scale solution, and Δh is the head drop along x_1. The upscaled hydraulic conductivities along other directions can be found in a similar manner by applying the appropriate boundary conditions. Equation (2-2) shows that the main idea behind this upscaling scheme is to preserve the average flux in the coarse block after upscaling. The basic assumption is that the flow is essentially linear (i.e., the large-scale head gradient is approximately constant over the target region). This is not valid in the near-well region, where the pressure head is proportional to the logarithm of the radial distance from the well (Durflosky, 2005).

A common concern related to the hydraulic conductivity upscaling is the smearing of preferred flow paths as a result of upscaling, which can lead to inaccurate prediction of plume transport. Flow-based gridding, in conjunction with accurate upscaling procedures, has been proposed as a more appropriate technique for generating coarse-scale models that retain the geologic realism of the fine-scale model (e.g., Wen, et al., 2003). The flow-based grid generation preserves high levels of resolution in regions of high flow and allows coarser resolution in regions of low flow. This can be especially important in and around geologic features, such as flow-conducting faults or buried channels. For reference, the present Yucca Mountain site-scale saturated zone flow models adopts an equivalent continuum approach to model faults, where the flow-conducting faults are conceptualized as vertical faults with higher hydraulic conductivities. The fault hydraulic conductivities were obtained through model calibration.

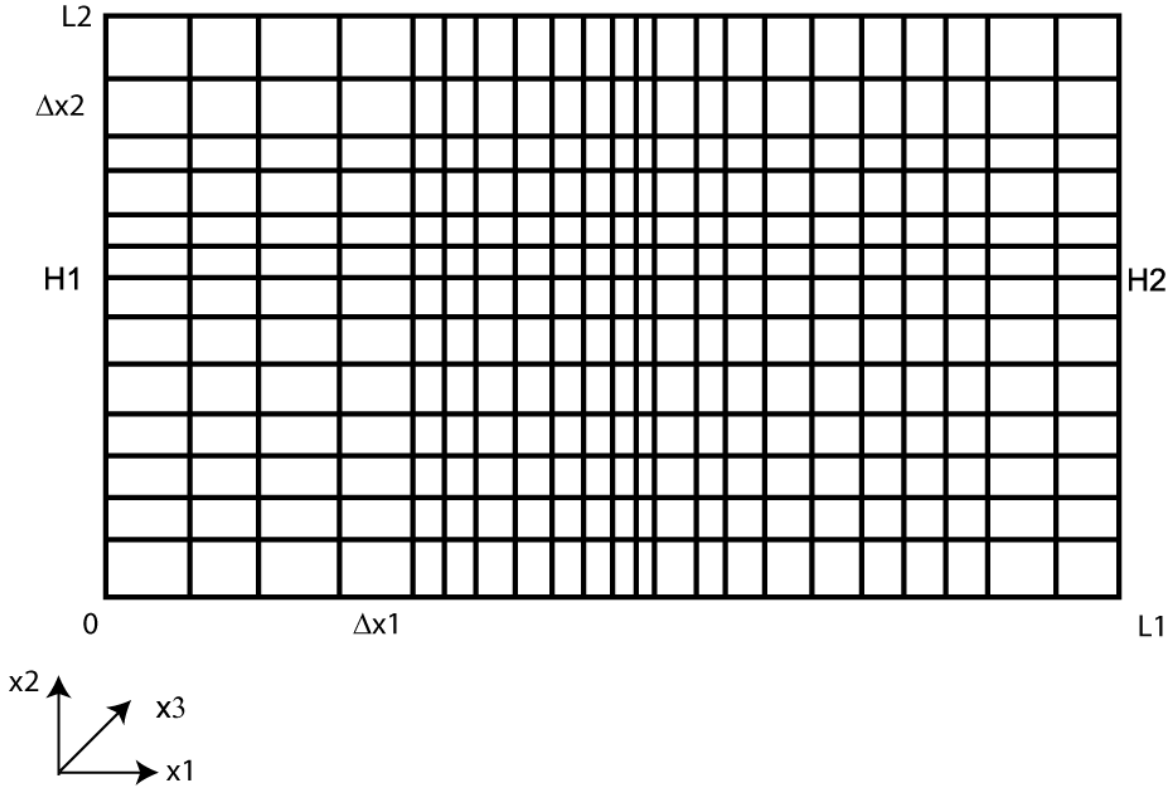

Figure 2-2. Illustration of the Flow-Based Hydraulic Conductivity Upscaling Technique for a Two-Dimensional Block. Shown is Problem Setup for Upscaling Conductivity in the x_1 Direction. No-Flow Boundaries Are Imposed on the Top and Bottom of the Domain and Constant-Head Boundaries Are Imposed on the Left and Right Side of the Domain. L_1 and L_2 Are the Length and Width of the Domain, Respectively. Δx_1 and Δx_2 are Dimensions of Each Grid Cell, Which Can Be Nonuniform.

2.4 Upscaling of Transport Parameters

The classic advection–dispersion equation is valid at a scale that is small compared to field-scale heterogeneity. Mathematically, it can be written as

$$\phi \frac{\partial C(\mathbf{x},t)}{\partial t} = -\nabla \cdot (\mathbf{q}(\mathbf{x})C(\mathbf{x},t)) + \nabla \cdot (\phi \mathbf{D}^{\ell} \nabla C(\mathbf{x},t)) \tag{2-3}$$

where C ($\mathbf{x}$,t) is aqueous-phase solute concentration, $\mathbf{q}$ ($\mathbf{x}$) is Darcy flux, ϕ is porosity, and $\mathbf{D}^{\ell}$ is the local hydrodynamic dispersion tensor defined as

$$\phi D_i^{\ell} = \phi D_d \varepsilon + \alpha_i |\mathbf{q}|, i = 1,2,3 \tag{2-4}$$

where D_d is the coefficient of molecular diffusion, ϵ is the tortuosity, D_i^{ℓ} are the eigenvalues of $\mathbf{D}^{\ell}$, and α_i are the local dispersivity coefficients. Just like the block hydraulic conductivity is used to preserve the average flux, the block equivalent dispersivity is used to preserve solute spread at the coarser scale. Thus, the block dispersion tensor $\mathbf{D}^b$ needs to include not only the hydrodynamic dispersion at the fine scale, but also an additional term to account for the loss of spreading caused by the suppression of subgrid information (Fernàndez-Garcia and Gómez-Hernández, 2007).

$$\phi D_i^b = \phi D_d \varepsilon + (\alpha_i + A_i^b)|\mathbf{q}|, i = 1,2,3 \quad (2\text{-}5)$$

where A_i^b is an additional term introduced to enhance the dispersivity at the numerical block scale. By definition, A_i^b is constant in time but can vary among different numerical blocks.

There is debate about whether or not the classical advection–dispersion equation can be upscaled to predict effective dispersion of reactive solutes. Classical macrodispersion theory is based on the first-order stochastic theory (e.g., Dagan, 1989; Gelhar, 1993) which shows that the macrodispersivity increases with time under steady-state flow conditions in a statistically stationary medium of finite correlation length. The solute resident time distribution at any given distance from the source can then be obtained by solving the advective–dispersion equation with the time-dependent macrodispersivity value. Wen and Gómez-Hernández (1998) showed that classical macrodispersion theory is not appropriate for transport in non-multi-Gaussian random hydraulic conductivity fields with enhanced connectivity, where the mass transport residence time distribution can be considerably different from that described by the analytical macrodispersion expressions. The well-connected flow paths resulted in earlier breakthroughs than those predicted by models based on the multi-Gaussian random field assumption. Liu, et al. (2004) further confirmed that solute transport in well-connected channel network systems can be highly asymmetric, with little solute dispersed upstream of the plume center and extensive downstream spreading of low concentrations. In other words, the breakthrough curves are skewed in such channelized systems.

The Fortymile Wash outcrop study conducted by Ressler, et al. (2000) suggests that the more permeable braid-belt bars are interbedded with the less permeable paleosol facies. The braid-belt bars, where connected, may form fast flow paths for radionuclides. As mentioned at the beginning of this chapter, one of the main focuses of this report is to study the effect of heterogeneity at the fine scales on the numerical block scale. Quantification of the effect of facies heterogeneity requires a fine-scale geologic model that honors plausible scenarios of facies distributions. The Markov chain model of facies transition probabilities developed by Sun, et al.[4] can serve such a purpose. The facies model also enables the linkage between facies heterogeneity and sorption heterogeneity.

Section 2.5 describes the block model generation process, while Section 2.6 discusses modeling of the physical and chemical heterogeneities. Particle tracking is used to model solute transport in the random fields. Appendix A briefly introduces the particle tracking code (SLIM-FAST) used in this report as well as some validation results.

[4]Ibid.

2.5 Generation of the Block Model

A block model is generated in four steps:

- Generate facies distribution at Level II using Level II statistics listed in Table 2-1 and the TSIM module of T-ProGS.
- Generate facies distribution at Level I using Level I statistics listed in Table 2-1 and TSIM.
- Generate multiple standard Gaussian random fields with zero mean, unit variance, and the ln$K$ correlation lengths listed in Table 2-1. The sequential Gaussian simulator in GSLIB is used for this purpose.
- Map facies distributions to K distributions.

For each facies type in each level of the hierarchy, a standard Gaussian random field is scaled according to the ln$K$ statistics of the facies and then assigned to all numerical cells belonging to that facies as governed by the facies random field. As a result, three standard Gaussian random fields are needed to generate one composite ln$K$ distribution in a block model: one for the paleosol facies and two for the open framework gravel and the nonopen framework gravel. A similar composition technique has been employed by Lu and Zhang (2002) for generating two-dimensional, bimodal hydraulic conductivity random distributions. The chemical heterogeneity is simulated by using the lnK_d statistics, which is detailed in the next section.

2.6 Coupling of Physical and Chemical Heterogeneities

It is well recognized that reactive transport at the field scale is affected by both the hydraulic and physico-chemical aquifer heterogeneities. In general, the mass transfer rate between solid and aqueous phase is controlled by the type of minerals, the quality, type, and distribution of organic matter; the geometry and composition of surface coatings, and the composition and distribution of facies (Haggerty and Gorelick, 1998). Existing methods for studying the coupled effects of physical and chemical heterogeneities are either hydraulic conductivity oriented or facies oriented. The former method generates correlated random fields of K and K_d directly (Bellin, et al., 1993; Bosma, et al., 1993; Painter, et al., 2001; Carle, et al., 2002); whereas the latter approach relies on a sedimentary architecture or a facies model to control the variability of K and K_d (Allen-King, et al., 2006, 2002,1998). Within each rock facies, the hydraulic and reactive transport properties may be considered constant or described by statistical properties. A positive ln$K$–lnK_d correlation reduces solute spreading compared to nonreactive tracers, whereas negative ln$K$–lnK_d correlation enhances solute spreading. However, field data are rarely available for validating the correlation between K and K_d for radionuclides or the mapping between facies types and K_d values.

Experiments suggest that the magnitudes of actinide sorption are the same for different minerals if normalized to an effective surface area (e.g., Bertetti, et al., 1998). Thus, the distribution of surface area normalized distribution coefficient {K_A [M^3/L^2] }which is related to K_d [L^3/M] as

$$K_d = K_A A \tag{2-6}$$

is modeled instead, where A is the effective surface area of a substrate. The retardation coefficient is defined as

$$R = 1 + \frac{\rho_b K_d}{\theta} \tag{2-7}$$

where ρ_b [M/L^3] is bulk density and θ [–] is porosity. The sorption of radionuclide Np-237 is used in this study as an example, and only those data pertaining to the site-scale model were selected for the statistical analysis. The detailed information of the 74 Np-237 K_A values for this study can be found in Appendix B, which shows that a number of the samples were taken from wells drilled as part of the Nye County Early Warning Drilling Program. The full chemistry data set and its sources are described elsewhere in Bertetti, et al. (2004, Section 3.1.1).

Figure 2-3 shows a map of the 74 Np-237 K_A sample locations in which the size of each circle is proportional to the magnitude of K_A. Each K_A represents the averaged value over the borehole depth. Histogram analysis suggests that K_A can be modeled by a lognormal probability distribution. This can be further seen from Figure 2-4, where the cumulative distribution of the raw lnK_A (circles) is fitted by a Gaussian cumulative distribution (solid line). The geometric mean of K_A is 2.03 mL/m^2 [6.37 × 10^{-3} oz/ft^2].

To investigate the spatial correlation among lnK_A data, two sets of variogram analyses were performed. In the first analysis, all 74 data were used to construct the lnK_A sample variogram, whereas in the second analysis, only data located south of UTM-Y = 4.07 × 10^6 m [1.33 × 10^7 ft] and thus close to the Fortymile Wash alluvial aquifer were used. In general, it is difficult to directly characterize lateral spatial variability of geologic/geochemical attributes because (i) lateral coverage of boreholes is usually sparse; (ii) the heterogeneity within geologic formations, such as alluvial deposits, is controlled by irregular depositional processes that are difficult to track laterally and (iii) the lateral direction is not necessarily horizontal or parallel to the ground surface (Carle, et al., 2002).

Figure 2-5 shows the omnidirectional lnK_A sample variogram constructed from the first analysis, and the exponential variogram model with a correlation length of 300 m [984 ft] and sill of 0.155 fitted to the data. Figure 2-6 shows the omnidirectional lnK_A sample variogram constructed from the second analysis, the exponential variogram model with a correlation length of 300 m [984 ft] and sill of 0.12 fitted to the data. The sample variograms are relatively noisy in both cases, and spatial correlation at smaller scales {< 1,000 m [3,280 ft]} is poorly characterized.

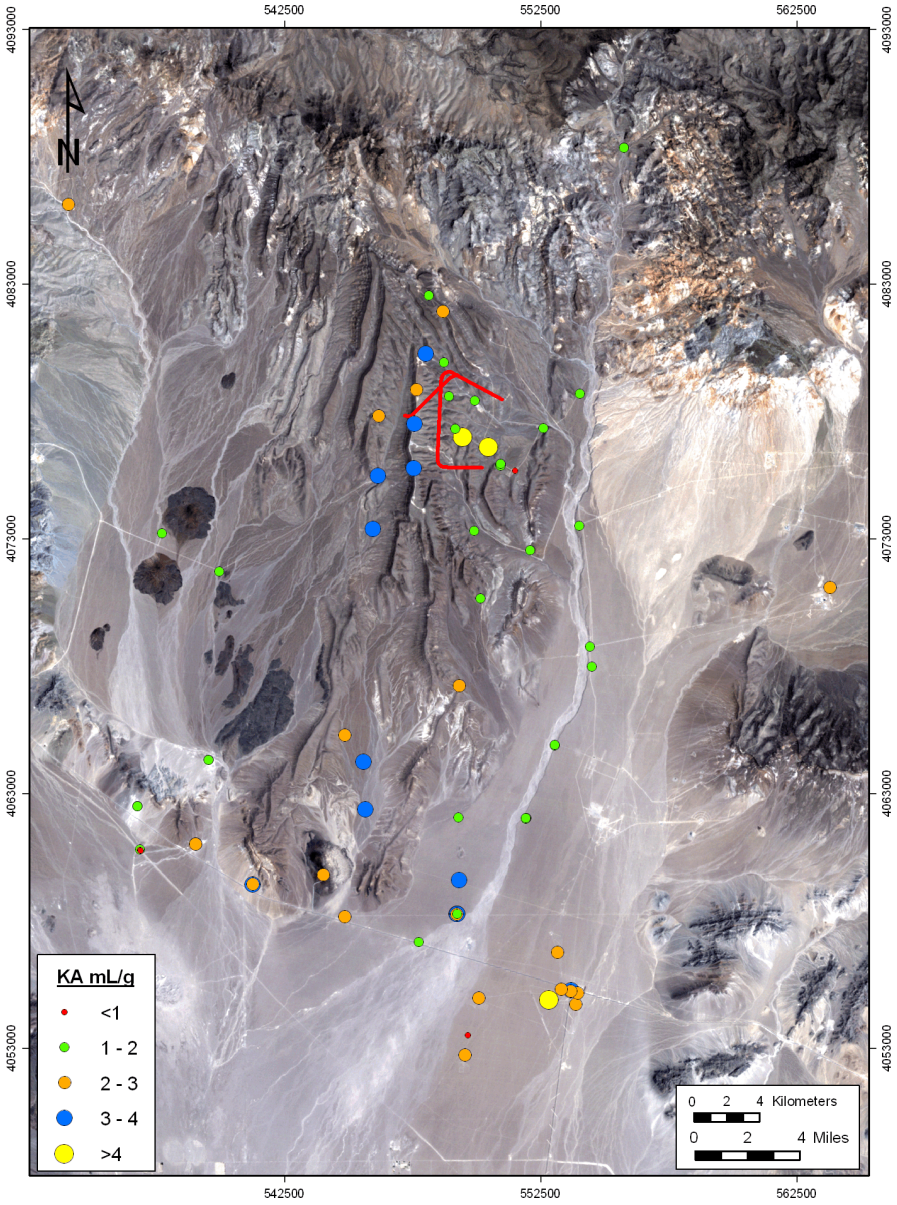

Figure 2-3. Map of the 74 Np-237 K_A Sample Locations. The Background Map Is a Satellite Image of Yucca Mountain Vicinity. All Data Were Collected From Wells Located Within the Extent of the DOE Saturated Zone Site-scale Model. The Sizes of the Symbols Are Proportional to the K_A Value. Coordinate Projection Is in Universal Transverse Mercator, Zone 11, North American Datum of 1983, Meters [1m = 3.28 ft]. More Information About the K_A Data Can Be Found in Appendix B.

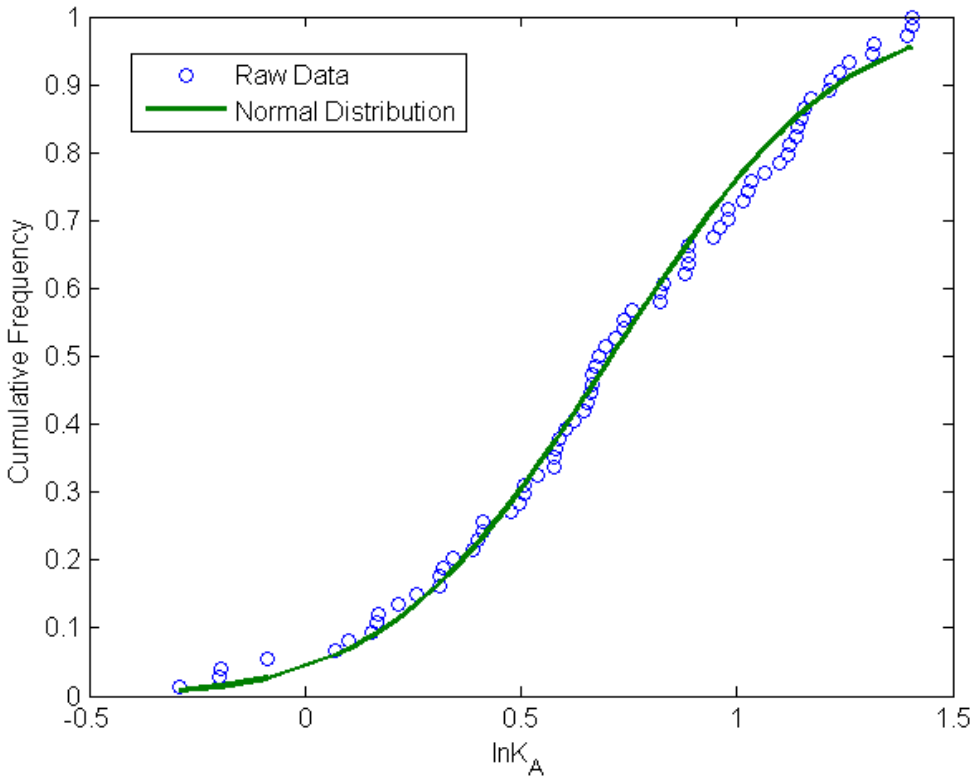

Figure 2-4. Cumulative Distribution of the Log-Transformed K_A Data (Circles), Which Can be Well Described by a Gaussian Distribution Function (Solid Line). The Units of the K_A Data Are in mL/m^2 [3.14x10^{-3} oz/ft^2].

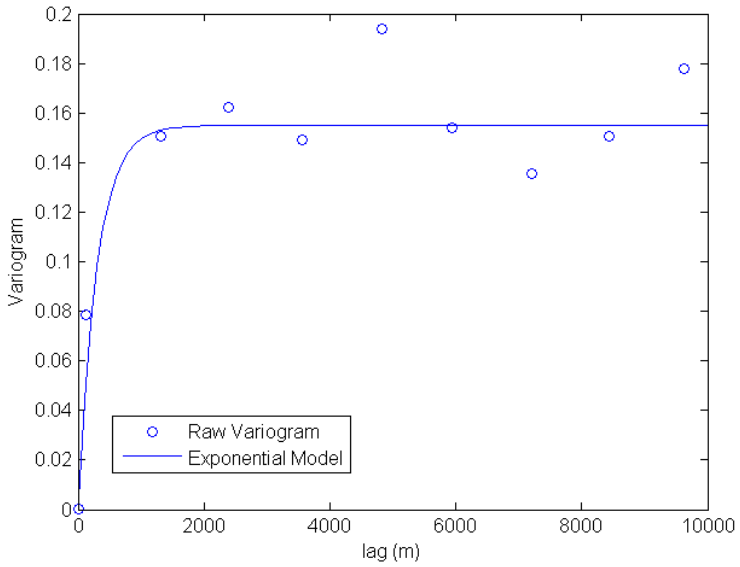

Figure 2-5. The lnK_A Sample Variogram Constructed Using the Whole K_A Dataset and a Fitted Exponential Variogram Model With a Correlation Length of 300 m [984 ft] and Sill of 0.155. The Unit of X-Coordinate Is m [1m = 3.28 ft].

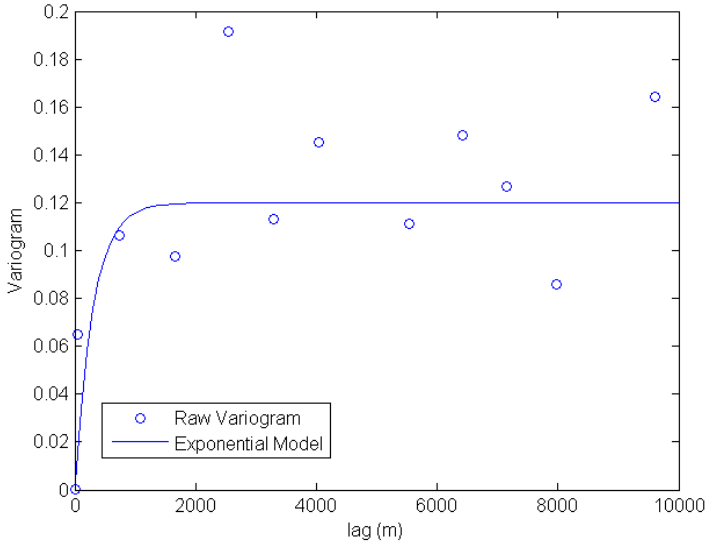

Figure 2-6. The lnK_A Sample Variogram Constructed Using a Subset of K_A Data That Are More Relevant to the Fortymile Wash Alluvial Aquifer. An Exponential Variogram Model With a Correlation Length of 300 m [984 ft] and Sill of 0.12 Is Fitted to the Sample Variogram. The Unit of X-Coordinate Is m [1m = 3.28 ft].

The poor fits suggest that there is either little correlation among $\ln K_A$ data at the scale considered in this study or the data are too sparse to reveal the underlying correlation. From their analyses of Frenchman Flat alluvium K_d geostatistics, Carle, et al. (2002) reported that spatial variation of the abundances of sorbing and nonsorbing minerals within mineralization zones (which partly correspond to alluvial layers) was largely attributed to microscale variability or nugget effect. As a result, the $\ln K_A$ data will be sampled from a truncated normal distribution with mean 0.709, standard deviation 0.41, and a range from −0.291 to 1.408.

The total surface area can be estimated experimentally using the N_2–BET method. Results can vary from study to study, depending on grain size, how the mineral was prepared, outgassing of the sample prior to measurement, and how long the mineral was allowed to age (Yates, 1975). Previous surface area analyses indicate that clays, which occur primarily as detrital and infiltrated matrix and authigenic grain coatings in the alluvium, dominate the surface area available for sorption of radionuclides passing through the alluvium (Bertetti, et al., 2004). Many of the Nye County Early Warning Drilling Program wells were drilled using rotary drilling methods. Notable exceptions are wells NC–EWDP–19PB and NC–EWDP–22PC, which were drilled using a sonic coring technique: a process during which the detrital matrix and authigenic cements holding grains and rock fragments together may be disrupted, but not removed or lost. Therefore, unlike well cuttings that contain sediments which have undergone varying degrees of desegregation (i.e., separation into component parts), loss, and potential contamination during the drilling process, the sonic core samples are more representative of the alluvial sediment mineralogy. Bertetti, et al. (2004) estimated mean effective surface area to be 12.1 m^2/g [3,690 ft^2/oz] with a range from 6.7 to 18.8 m^2/g [2,040 to 5,730 ft^2/oz] based on sonic cores collected from NC–EWDP–19PB. They also suggested that effective surface area be sampled from a uniform range of 1.9 to 12.1 m^2/g [580 to 3,690 ft^2/oz] to incorporate the lowest measured values for alluvium while accommodating the higher surface areas indicated by the NC–EWDP–19PB.

Given the limited quantitative information that can be used to link facies distributions to clay contents and subsequently to surface areas, uniform distributions are assumed for surface areas. The paleosol facies (Level II) is expected to have the highest clay content on average, while the open framework gravel facies (Level I) has the lowest. Thus, for each realization, the $\ln K_A$ distribution is generated by the sequential Gaussian simulator and the effective surface area distribution is obtained by randomly sampling the uniform distribution assigned for each facies. As a result, the resulting K_d distribution (product of surface area and K_A) is also log-normal. Although no explicit correlation between K_d and K is assumed, the two are linked via the surface areas, which are assumed different for different facies. The hypothetical uniform distributions assumed for different facies are given in Table 2-2.

Table 2-2. The Hypothetical Statistics of the Effective Surface Area (A) for Different Hydrofacies

Facies Type	Mean A (m^2/g)*	Range of A (m^2/g)
Paleosols	10.0	[8, 12]
Non-OFG	6.0	[2, 10]
OFG†	2.0	[1, 3]

*1 m^2/g = 305 ft^2/oz
†OFG = Open framework gravel

3 RESULTS AND DISCUSSION

3.1 Problem Setup

The dimensions of the three-dimensional block model are 300 x 300 x 20 m [984.3 x 984.3 x 65.6 ft]. The domain of a three-dimensional block is discretized uniformly into 2 x 2 x 0.4-m [6.6 x 6.6 x 1.3-ft] numerical cells. The fine resolution is necessary to capture the variability of Level I facies.

The properties of the block model were generated according to the procedure described in Section 2.5. The quality of the random fields generated by TSIM was checked by comparing the ensemble mean and variance with the specified mean and variance and by comparing the variograms with the analytical, exponential variogram model for binary facies

$$\gamma(h) = \sigma_I^2 \left[1 - \exp(-h / \lambda_I)\right] \tag{3-1}$$

where h is separation distance, the variance $\sigma_I^2 = L_1 L_2 / (L_1 + L_2)^2$, the correlation length $\lambda_I = L_1 L_2 / (L_1 + L_2)$, and L_1 and L_2 are the mean lengths of the two facies. The quality of the standard Gaussian random fields generated by the sequential Gaussian simulator was checked in a similar manner.

Constant head boundaries of 100 and 99.7 m [328 and 327 ft] are imposed on *y* faces of the model so that the mean hydraulic gradient is 0.001 along the *x* direction. The magnitude of the mean hydraulic gradient is within the range of flow conditions observed in the Fortymile Wash alluvial aquifer (Bechtel SAIC Company, LLC, 2004). All other faces of the model are subject to no-flow boundary conditions. The anisotropy ratio between horizontal and vertical hydraulic conductivity is set to 10.

For particle-tracking simulation, a planar source is placed perpendicular to the mean flow direction. The dimensions of the planar source are 1 x 220 x 4 m [3.3 x 721.8 x 13.1 ft], and the coordinates of its centroid are 45.5, 150, and 10 m [149.3, 492.1, and 32.8 ft]. For each simulation, 10,000 particles were released from the source at time 0. Molecular diffusion and pore-scale dispersion are ignored in particle tracking. The total number of realizations used in the Monte Carlo simulation is 50, which was sufficient to produce a good match to the analytical solutions during validation testing (see Appendix A). Note that a large initial plume size is needed to diminish the effect of plume size on macrodispersivity.

Three test cases were used to demonstrate the effects of physical heterogeneity on conservative tracer transport. The main differences in the three test cases are in the ln*K* variances of Level I facies (Table 3-1).

The variances are smallest in Case 1, but increase significantly in Cases 2 and 3. Thus, Case 1 serves as a baseline case, whereas Cases 2 and 3 test sensitivities to ln*K* variances. Figure 3-1 presents two examples of Level I facies distributions that were generated using TSIM, showing that the more permeable open framework gravel facies are embedded in the less permeable nonopen framework gravel facies. Figure 3-2 shows three examples of the

Table 3-1. ln*K* Statistics of the Level I Hydrofacies for the Three Test Cases				
Case No.	**$\langle \ln K_1 \rangle$***	**$\langle \ln K_2 \rangle$**	**σ_1^2**	**σ_2^2**
1	2.51	0.21	0.1	0.1
2	2.51	0.21	1.0	0.5
3	2.51	0.21	4.0	1.0
*Subscript 1 = open framework gravel; subscript 2 = nonopen framework gravel				

composite *K* random fields generated by combining Level II facies distribution with Level I facies distributions. The three examples represent realizations from the test cases 1 to 3. Figure 3-2 shows that the high-conductivity zones tend to be more connected and form more contiguous paths as the ln*K* variance increases.

The sample ln*K* histograms for test cases 1 to 3 are shown in Figure 3-3 (a) to (c), respectively. The bimodal pattern of ln*K* distribution can be most clearly seen from Figure 3-3(a). As the variance of ln*K* distribution increases, significant overlaps develop between the two ln*K* distributions.

3.2 Hydraulic Conductivity Upscaling

The upscaled (or equivalent) block K_b was obtained using the flow-based upscaling procedure described in Section 2.3, where the mean hydraulic gradient of 0.001 was substituted in Eq. (2-2) to calculate the equivalent block hydraulic conductivity, K_b. The ensemble mean and standard deviations of K_b were calculated along the *x* direction, and the results are listed in Table 3-2 for the three test cases.

Table 3-2. Mean and Standard Deviation of the Upscaled Hydraulic Conductivity (K_b) for the Test Cases. The Results Are for the *x* Direction.		
Case No.	**$\langle K_b \rangle$ (m/day)***	**σ_b (m/day)**
1	2.21	0.04
2	2.35	0.10
3	2.58	0.18
* 1 m = 3.28 ft		

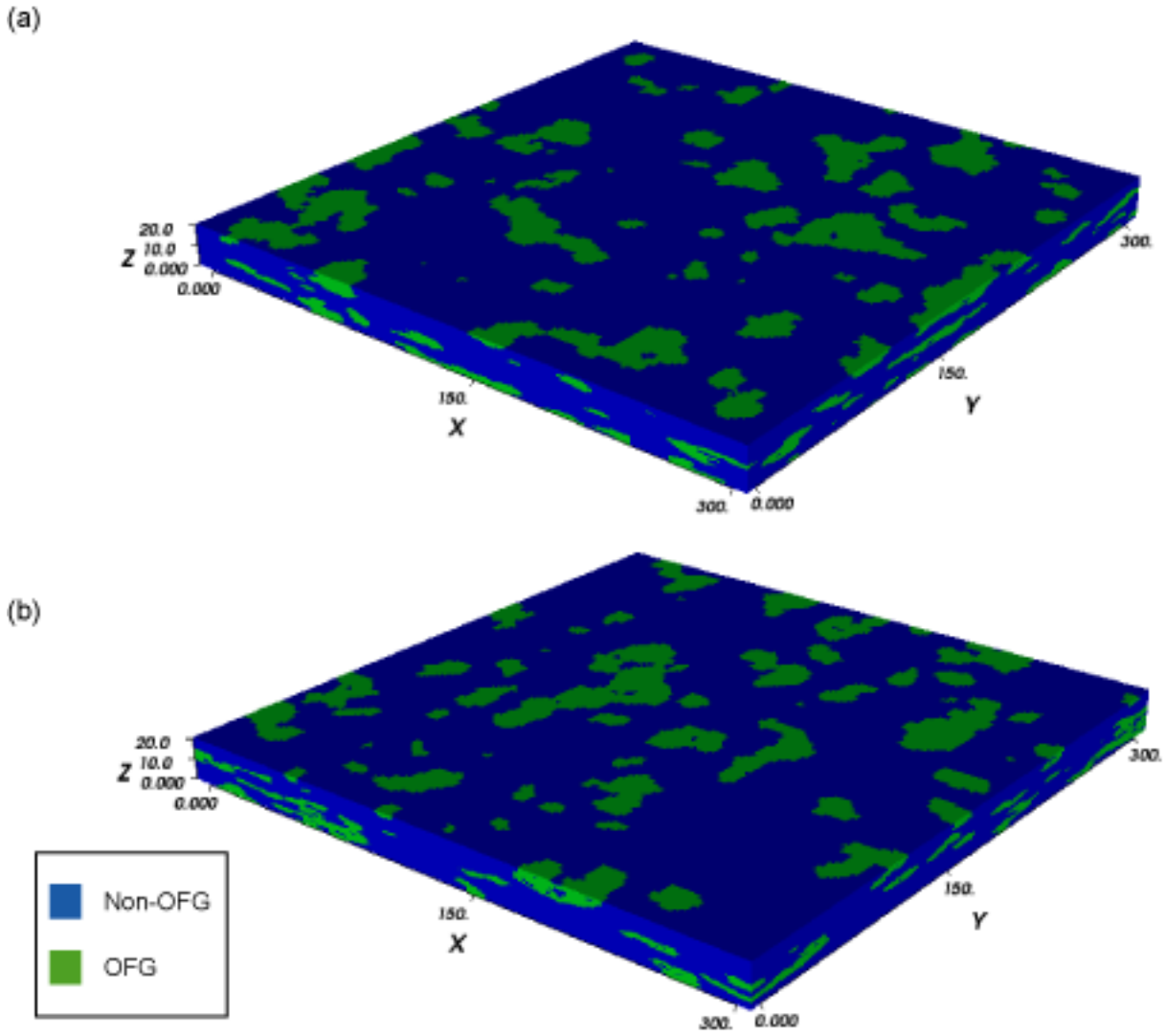

Figure 3-1. Examples of the Level I Facies Distributions Generated by TSIM. Level I of the Hierarchical Fortymile Wash Alluvium Model Consists of Two Facies: the Open Framework Gravels (Volume Fraction = 0.2) and NonOpen Framework Gravels (Volume Fraction = 0.2). The Units of Coordinates Are in m [1m = 3.28 ft].

(a)

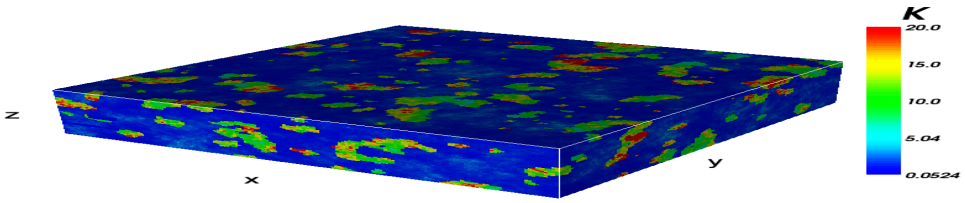

(b)

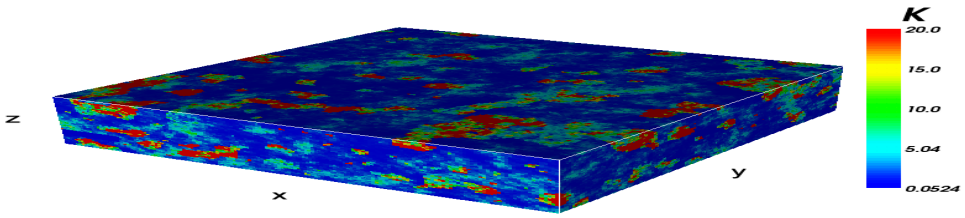

(c)

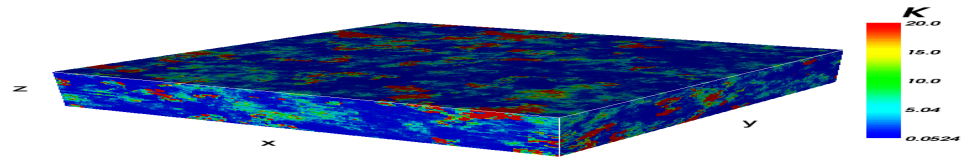

Figure 3-2. Examples of the Composite *K* Random Fields Generated by Merging Level II Facies Distribution with Level I Facies Distributions. Shown in (a) to (c) Are Sample Realizations from Case 1 to 3, Respectively. The Domain Size Is 300 x 300 x 20 m [984x984x66 ft]. The Units of *K* Are in m/day [3.28 ft/day]. To Ease Visualization, the Upperlimit of the Scale Bar Is Set to 20.0 m/day [66 ft/day] for all Cases and the Vertical Exaggeration Ratio Is 3.0.

The block hydraulic conductivity values assigned to the valley-fill alluvial aquifer unit are 4.76 m/day [15.6 ft/day] in the DOE site-scale saturated zone flow model (Bechtel SAIC Company, LLC, 2004, Table 6-22) and 3.0 m/day [9.84 ft/day] in the NRC site-scale saturated zone flow model (Winterle, 2003). Ensemble mean block conductivity values are close to the hydraulic conductivity values in the current site-scale models. In general, an increase in Level I ln$K$ variance leads to an increase in the ensemble block conductivity variance. However, the increases in ensemble block conductivity variances are relatively small, given significant increases in ln$K$ variances of individual facies. This is direct evidence of information loss in the course of upscaling. In other words, upscaling hides the heterogeneity existing at the subgrid scales.

The values of block conductivity along other directions were not calculated. The block hydraulic conductivity values along y direction are expected to be the same because of the isotropic correlation structure adopted in this study. The vertical block conductivity is smaller because an anisotropic ratio of 10 was used when generating the composite conductivity fields.

3.3 Nonreactive Transport

The macrodispersivity can be derived from the second-order moments of solute plumes, which are represented in this context by a set of particles

$$A_i = \frac{1}{2U}\frac{dX_{ii}}{dt} \quad (i = 1,2,3) \tag{3-2}$$

where A_i are the macrodispersivities, U is the mean particle velocity in the main flow direction, and X_{ii} are single particle displacement autocovariances. Only under the condition of ergodicity are X_{ii} equivalent to the ensemble mean of the second-order spatial moments of concentration plumes (Dagan, 1989). In this report, the following expressions for ensemble macrodispersivities are used (Fernàndez-Garcia and Gómez-Hernández, 2007)

$$A_1 = \frac{1}{2U}\frac{d\left(\langle S_{11}\rangle + R_{11}\right)}{dt}, \qquad A_i = \frac{\langle \Psi_{ii}\rangle + R_{ii}}{2x} \quad (i = 2,3) \tag{3-3}$$

where $\langle\cdot\rangle$ is the ensemble average operator, x is the x_1 coordinate of a control plane (or monitoring plane), S_{11} is the second central moment of particles around the center of mass (or plume centroid), R_{11} is the variance of the center of mass over all realizations, Ψ_{ii} are the variances of the differences between the transverse particle displacements and their release locations. In the literature, the quantities Ψ_{ii} have been used as surrogates for X_{ii} because of difficulties related to directly calculating transverse moments in strongly heterogeneous media (Wen and Gómez-Hernández, 1998; McKenna, et al., 2003). Note that Eq. (3-3) is for purely advective transport. If pore-scale dispersion and molecular diffusion are included, an additional term needs to be added to the right-hand side of the equation. It is well known that pore-scale dispersion and molecular diffusion can contribute to enhanced mixing along and across streamlines. In regions of stagnant flow, diffusion provides the only mechanism for particles to exit such regions.

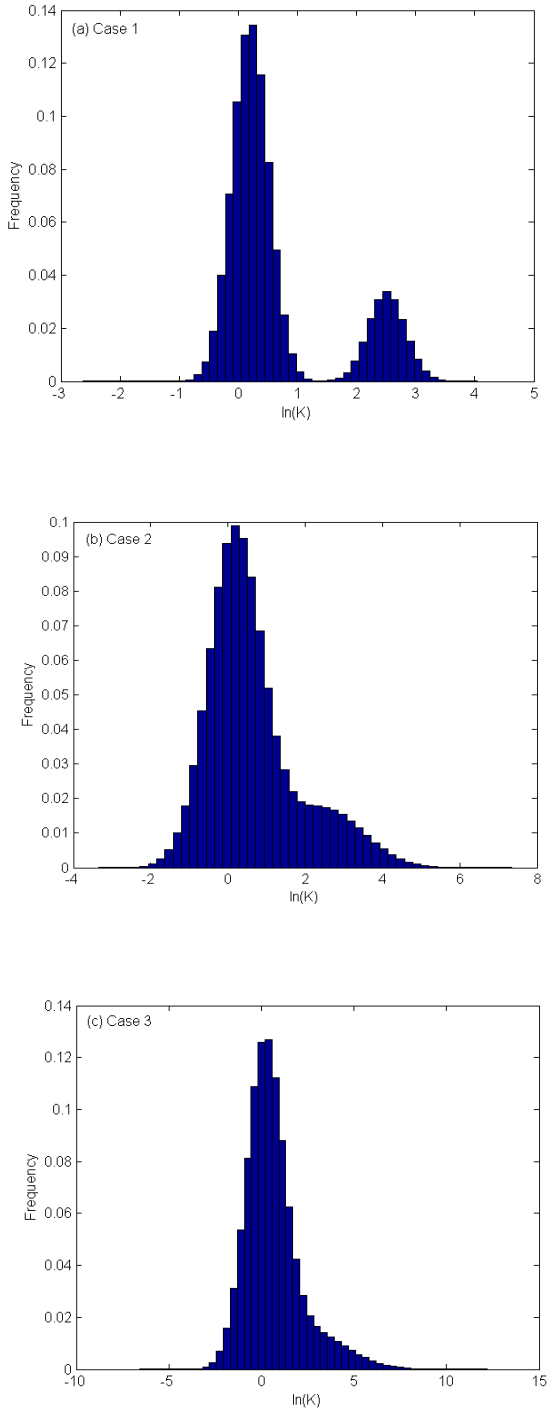

Figure 3-3. Histograms of the Composite Log Hydraulic Conductivity Fields for Test Cases 1 to 3. The Composite Random Fields Are Generated According to the Procedure Described in Section 2-5. The Bimodal Nature of the Histograms Can Be Observed From the Figures.

In Figures 3-4(a) to (c), the calculated macrodispersivities are shown as a function of travel distances from the planar source for Cases 1 to 3. The last control plane was set at x_1 = 50 m [164 ft] to avoid biases introduced by particle losses through the flow boundary. Alternatively, the temporal moments of first particle arrival time can be calculated and the macrodispersivities can be calculated according to Wen and Gómez-Hernández (1998). For comparison purposes, the analytical solutions derived by Dai, et al. (2004) based on first-order approximation were also calculated using statistics of Level I facies, where the volume proportions and the mean ln*K* of the two facies are given in Table 3-1, and the ln*K* variances are assumed to be the same as those used in Cases 1 to 3. The analytical results of Dai, et al. (2004) for the special case of binary facies, are given as

$$A_1(\tau) = \sigma_Y^2 \lambda_I \left\{ 1 + \frac{4}{e^\tau \tau^4} \left[6(e^\tau - \tau - 1) - \tau^2 (e^\tau + 2) \right] \right\}$$

$$A_i(\tau) = \sigma_Y^2 \lambda_I \left\{ \frac{1}{e^\tau \tau^4} \left[12(1 + \tau - e^\tau) + \tau^2 (5 + e^\tau + \tau) \right] \right\}, i = 2,3 \tag{3-4}$$

where $\tau = tU / \lambda_I$ is the dimensionless travel time, and the ln*K* variance (σ_Y^2) and integral scale (λ_I) are defined as

$$\sigma_Y^2 = p_1 p_2 (m_1 - m_2) + p_1 \sigma_{Y,1}^2 + p_2 \sigma_{Y,2}^2$$

$$\lambda_I = p_1 \bar{\ell}_2 = p_2 \bar{\ell}_1 \tag{3-5}$$

in which m_i, $\sigma_{Y,i}^2$, $\bar{\ell}_i$ (i = 1,2) are the geometric mean, ln*K* variances, and mean lengths of each facies, respectively. It is emphasized that these analytical solutions are only for one level of facies hierarchies considered here, while the composite *K* fields used in the Monte Carlo simulation include heterogeneities related to both Level I and II facies.

Figure 3-4(a) shows that the simulated longitudinal dispersivity curves increase linearly at early travel times (i.e., short travel distances) and then increase slowly at later times. Only Case 1 seems to reach an asymptotic value of 7 m [23 ft] within the travel distance shown, while the longitudinal dispersivities in all the other cases continue to increase. The time for A_1 to reach the large-time asymptotic behavior can be related to facies volume fractions and correlation scales (Rubin, et al., 2006). In theory a plume only reaches its asymptotic behavior after it samples all heterogeneities at different spatial scales. This asymptotic regime is synonymous to the Gaussian transport regime in the classical theory on advection and dispersion. However, the time for a plume to reach the Gaussian regime can be exceedingly long in multimodal hydraulic conductivity fields, such as those considered in this report. The implication is that block dispersivities defined in Eq. (2-5) are scale dependent.

Recall that the lateral mean lengths of the Level II facies are on the order of 1,000 m [3,280 ft]. Thus, all A_1 may not reach asymptotic values at the block scale, but are mainly a manifestation of the effects of subgrid heterogeneities. The question of whether or not the large scale heterogeneity present at Level II can be captured by the coarse-grid model largely depends on how well the upscaled conductivity field preserves the large scale correlation structure.

Figure 3-4(a) also shows that the analytical solutions capture the general trends in all cases, suggesting subgrid dispersivity is dominated by Level I facies at the block scale of this study.

The transverse dispersivities exhibit different behaviors from the analytical solution at large times, although the climbing portion and the peak value match well with the analytical solution. There are two potential causes for the simulated transverse dispersivity continual growth. One is related to the approximate nature of Eq. (3-3) for calculating transverse dispersivities. The other is related to the fact that two levels of facies are involved in the simulation, whereas the analytical solution only considers one level of the hierarchy. From the curves it can be estimated that the ratios between simulated longitudinal macrodispersivty and the horizontal and vertical dispersivities are around 20 and 300, respectively.

3.4 Reactive Transport

Random realizations of K_d distributions were generated according to the methodology and K_d statistics described in Section 2.6. Figure 3-5 shows an example of the resulting composite K_d realizations. Although no explicit correlation between K and K_d is assumed, the spatial pattern of K_d generally correlates with the facies distributions as a result of sampling from different surface area distributions assigned to the facies. The discrete dots reflect the overlapping of surface area ranges and the lack of spatial correlation among K_d values. Figure 3-6 shows the sample histogram of the $\ln K_d$ distribution from which the bimodal nature of the K_d distribution can be seen. The ensemble geometric mean of all generated $\ln K_d$ realizations was calculated to be 0.0047 m^3/kg [0.0047 ft^3/oz]. The bulk density of the alluvium material is 2,000 kg/m^3 [125 lb/ft^3] by assuming the solid density of 2,500 kg/m^3 [156 lb/ft^3] and porosity of 0.2; thus the geometric mean of the retardation coefficient R is 48.

Reactive particle tracking was performed using the generated K_d fields and the flow fields obtained for Cases 1 to 3. The resulting dispersivity curves are shown in Figures 3-7(a) to (c), where the letter R in the case names indicates reactive transport. Comparing with the results for nonreactive cases shown in Figures 3-4(a) to (c), the results here indicate that sorption enhances the longitudinal spread, but the transverse dispersivities are little affected. The longitudinal dispersivity also shows a sharp increase after a short travel distance. These phenomena are consistent with previous observations in the literature, which are summarized in Rubin (2003, Chapter 10). Recall that the facies-based approach is used to model spatial heterogeneity of sorption parameters and the more permeable facies (e.g., open framework gravels) are conceptualized to have smaller surface areas. As a result, the fast flow channels are coupled with low retardation and the low-conductivity zones are coupled with high retardation. Interestingly, the particle spread in Case 3R is similar to that of Case 2R. This is because the test cases differ mainly by the variances of the open framework gravels, which account for only a small proportion of the whole volume and are less sorptive compared with the less permeable nonopen framework gravels and the paleosols. Thus, increasing the hydraulic conductivity variances for both the open framework gravels and the nonopen framework gravels in case 3R may have suppressed solute spread, as compared to that in Case 2R.

(a)

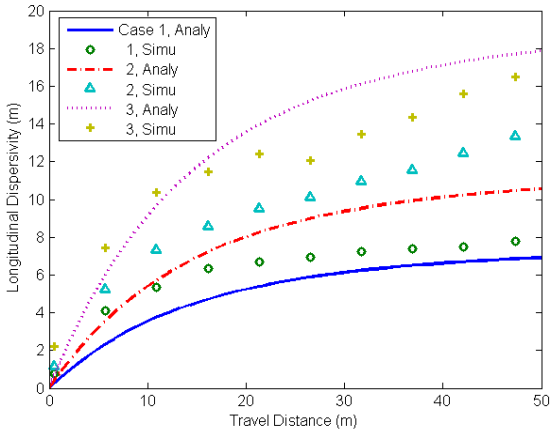

(b)

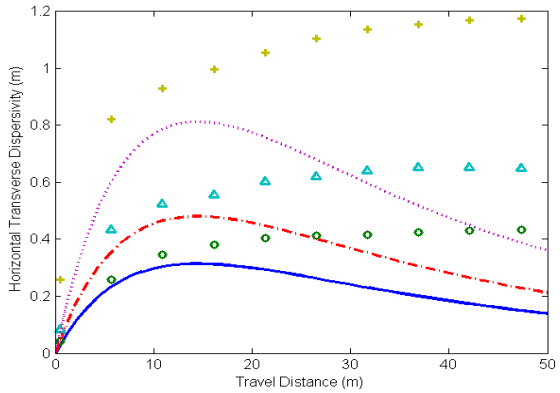

(c)

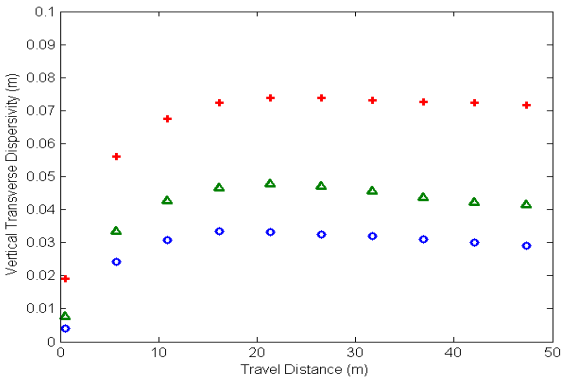

Figure 3-4. Macrodispersivities Calculated from Particle Displacement Statistics for Non-Reactive Tracer Transport. The Particle Displacement Statistics Were Obtained From Monte Carlo Simulation of Particle Movements in the Block Model: (a) Longitudinal Macrodispersivity Along the Main Flow Direction; (b) Transverse Macrodispersivity in the Horizontal Direction; and (c) Transverse Macrodispersivity in the Vertical Direction. Also Shown in (a) and (b) Are Analytical Solutions Derived by Dai, et al. (2004) for Particle Displacement in Bimodal Porous Formations [1m = 3.28 ft].

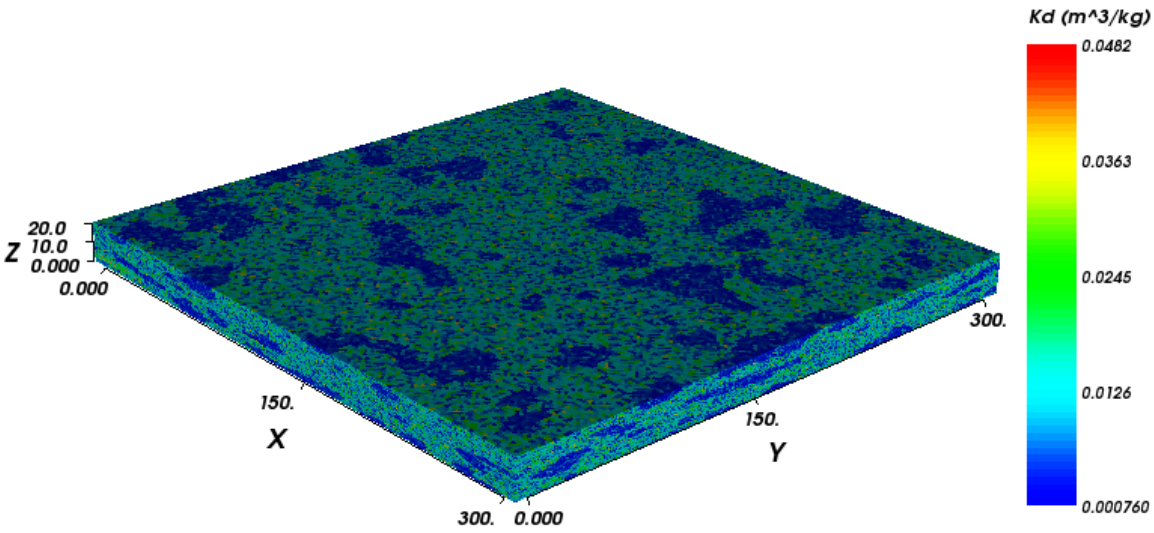

Figure 3-5. An Example of K_d Distribution. For Each Cell, lnK_A Is Sampled From the Truncated Normal Distribution and the Surface Area Is Sampled From Uniform Distributions. K_d Is the Product of the Two. The Coordinates Are in m [1m = 3.28 ft].

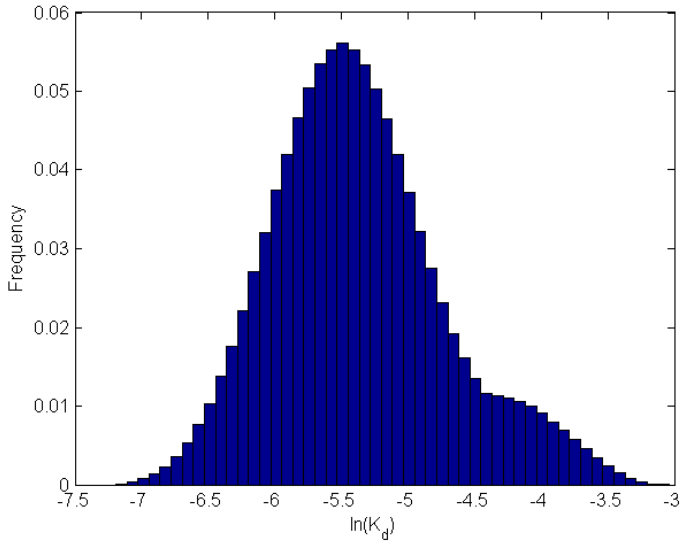

Figure 3-6. Histogram of the ln(K_d) Distribution, From Which the Bimodal Pattern Can Be Observed. The Unit of K_d Is in m^3/kg [1 m^3/kg = 16 ft^3/lb].

(a)

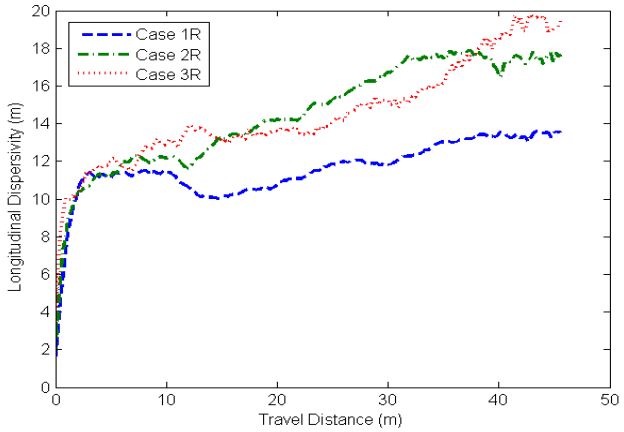

(b)

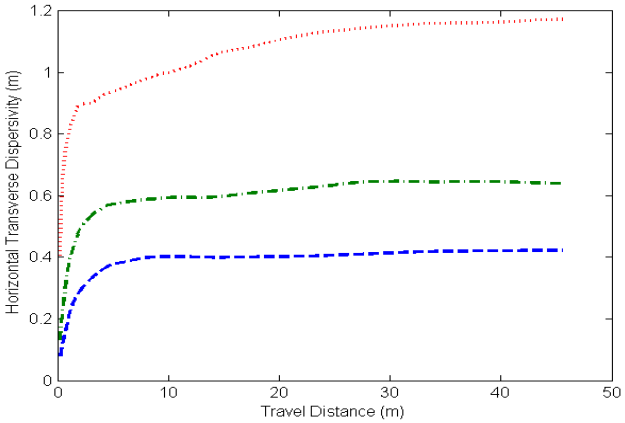

(c)

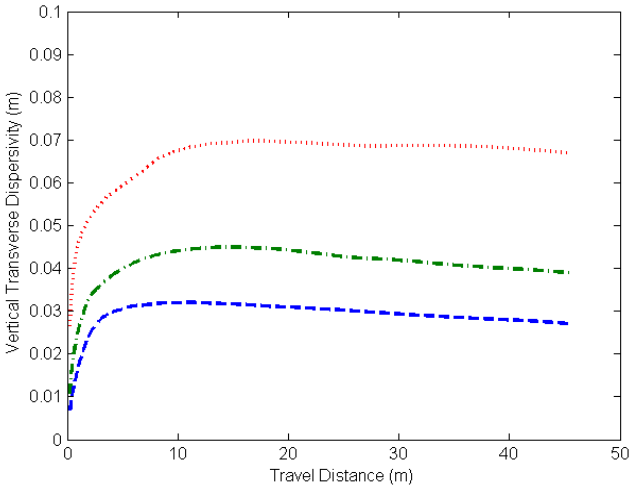

Figure 3-7. Macrodispersivities Calculated From Particle Displacement Statistics for Reactive Transport. The Flow Fields Are the Same as Those Used in Cases 1 to 3.

Two separate test cases were performed to quantify the sensitivity of plume spread to sorption heterogeneity. In the first sensitivity test, a constant K_d equal to its arithmetic mean was used in all realizations. The flow fields used are identical to those previously used in Case 1. The resulting longitudinal macrodispersivity is shown in Figure 3-8, along with results from Cases 1 and 1R. The results indicate that the chemical heterogeneity enhances solute spread and ignoring it may lead to underestimation of block dispersivity.

In the second sensitivity test, the effect of spatial correlation in K_A on plume spread was investigated. The variogram analyses on $\ln K_A$ data did not reveal significant correlation at the 500-m [1,640-ft] scale (see Figures 2-5 and 2-6). The data density, however, precludes meaningful variogram analyses at smaller lag spacings. It has been assumed so far that K_A is not autocorrelated. Now assume that K_A is autocorrelated at relatively short distances, and for illustration purposes, at the same correlation length as that of the $\ln K$ fields. A different set of K_A realizations was generated, and a Monte Carlo simulation was performed using the flow fields of Case 1. The result, shown in Figure 3-9, indicates that correlated K_A reduces longitudinal plume spread, as compared to that of no correlation assumed in Case 1R.

3.5 Flow Path Connectivity

A final note is on flow path connectivity. The macrodispersivity tensor, whose components were calculated using spatial moments of particle displacements, has been used as the primary measure for plume spread in this report. The moments of particle arrival time can provide another measure of the heterogeneous structure of porous formations. Most importantly, it can provide a measure of flow path connectivity. Recently, Knudby and Carrera (2005) compared several indicators for quantifying the degree of channeling (i.e., fast flow pathways) in porous media. The transport connectivity indicator, defined as the ratio between mean and early travel times (time at which 50 percent of the solute has arrived at the outlet), was identified as one of the effective indicators for indicating the presence of connected high-conductivity features. Examples of particle location snapshots are given in Figure 3-10, where particle movements in a random realization picked from Case 3 are shown for two different travel times. These snapshots of particle locations clearly show evidence of fast flow channels in the stochastically generated composite conductivity fields.

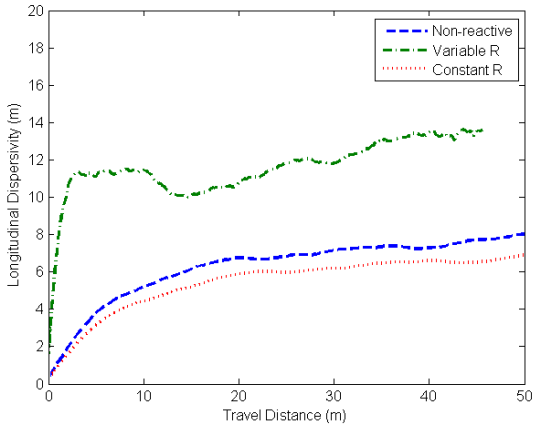

Figure 3-8. Comparison Between Longitudinal Dispersivity for Non-Reactive Transport, Reactive Transport With Constant K_d and Reactive Transport With Heterogeneous K_d, Using the Flow Fields of Case 1.

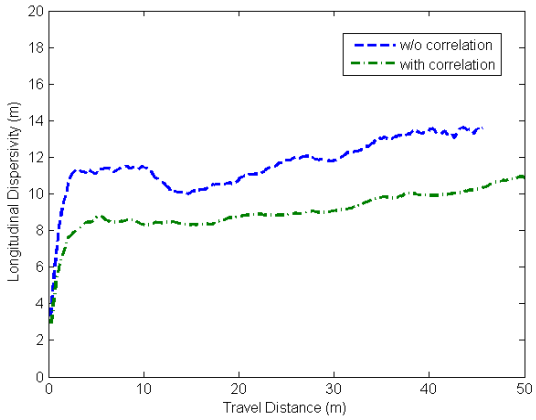

Figure 3-9. Comparison Between Longitudinal Dispersivity for Reactive Transport With Correlated K_d and Uncorrelated K_d, Using the Flow Fields of Case 1. For Illustration, the Correlated K_d Fields Are Assumed to Have the Same Correlation Structure as the ln$K$ Random Fields.

.

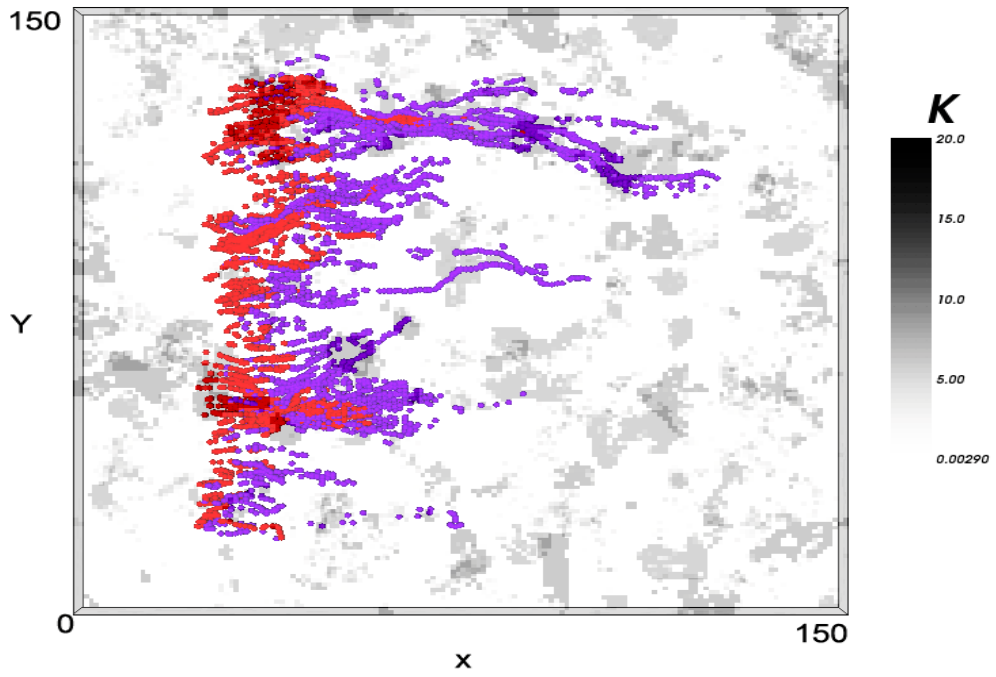

Figure 3-10. Plan View of Particle Locations at Time = 2,000 Days (Red) and 4000 Days (Purple). The Fingering of Solute Plume Can Be Clearly Seen From the Snapshots. The Hydraulic Conductivity Field Was Randomly Chosen From One of the Realizations Generated for Case 3.

4 CONCLUSIONS

Solute spread in natural geological formations is controlled by variations in hydraulic conductivity at a multiplicity of scales. The advection–dispersion equation with an uncertain dispersion coefficient is considered the most reasonable way to predict large-scale and large-time transport. Site-scale flow and transport models are often represented using coarse numerical grids because of computational limitations. The loss of subgrid information and variability can have a large-scale impact on plume mixing and movement. It is standard practice to obtain equivalent flow properties such as the hydraulic conductivity tensor through upscaling. However, performing transport using upscaled flow parameters may predict increased early arrival time and decreased late arrival time to the compliance boundary.

The alluvial aquifer of Fortymile Wash, Nevada, is conceptualized as a potential natural barrier to radionuclide transport. Currently, the valley-fill alluvial aquifer is modeled as a hydrogeologically homogeneous unit in the DOE and NRC site-scale saturated zone models. Neither the small- nor large-scale heterogeneity existing in the alluvium is explicitly taken into account. Previous theoretical and field studies conducted by CNWRA suggested that saturated alluvium consisted of facies having distinctively different hydraulic and sorptive properties.

In this study, the concept of block dispersivity is explored to quantify the effects of physical and chemical heterogeneities in the alluvium. A block model having dimensions of a typical grid block in the Yucca Mountain site-scale saturated zone models is used. The flow properties of the model were generated stochastically using a hierarchical alluvium facies model developed based on boreholel cutting logs from Nye County Early Warning Drilling Program and outcrop studies. The Np-237 sorption parameters were extracted from a CNWRA chemical database that was developed based on samples collected from the Yucca Mountain vicinity. Variogram analyses of the K_A (surface area normalized sorption parameter) data did not reveal strong spatial correlation among the data and, thus, a truncated normal distribution was used to sample K_A distribution. A facies-driven approach was used to model surface area distributions in which different ranges of surface areas were assigned to different facies and the surface area of each cell was then sampled based on its facies type. Monte Carlo simulation was performed to obtain particle displacement statistics from a planar source and for different realizations of composite hydraulic conductivity and K_d distributions.

Flow-based upscaling indicates that the magnitudes of the mean block hydraulic conductivities are similar to the hydraulic conductivity values assigned to the valley-fill alluvial unit in site-scale models. The results of nonreactive transport indicate that longitudinal macrodispersivities can be on the order of 10 m [32.8 ft] or greater. The ratios between longitudinal and transverse dispersivities are around 20 in the horizontal direction and 200 in the vertical direction. The results of reactive transport indicate that retardation introduces at most a twofold increase in solute spread in the longitudinal direction. Additional sensitivity studies conducted using correlated K_A random fields indicate that correlation in K_A reduces plume spread. For example, with a correlation length of 10 m [32.8 ft], longitudinal dispersion increases only slightly over the unretarded case, consistent with the results of Painter, et al. (2001).

5 REFERENCES

Al-Aziz, E., S.C. James, B.W. Arnold, and G.A. Zyvoloski. "The Site-Scale Saturated Zone Flow Model for Yucca Mountain." Fall Meeting Supplement., Abstract H11D–1286. Vol. 87, No. 52. *Eos Transactions, American Geophysical Union*. 2006.

Allen-King, R.M., R.M. Halket, D.R. Gaylord, and MJ.L. Robin. "Characterizing the Heterogeneity and Correlation of Perchloroethene Sorption and Hydraulic Conductivity Using a Facies-Based Approach." *Water Resources Research*. Vol. 34. pp. 385–396. 1998.

Allen-King, R.M., P. Grathwohl, and W. P. Ball. "New Modeling Paradigms for the Sorption of Hydrophobic Organic Chemicals to Heterogeneous Carbonaceous Matter in Soils, Sediments, and Rocks." *Water Resources Research*. Vol. 25. pp. 985–016. 2002.

Allen-King, R.M., D.P. Divine, M.J. L. Robin, J.R. Alldredge, and D.R. Gaylord. "Spatial Distributions of Perchloroethylene Reactive Transport Parameters in the Borden Aquifer." *Water Resources Research*. Vol. 42, No. W01413. doi:10.1029/2005WR003977. 2006.

Attinger, S., M. Dentz, H. Kinzelbach, and W. Kinzelbach. "Temporal Behaviour of a Solute Cloud in a Chemically Heterogeneous Porous Medium." *Journal of Fluid Mechanics*. Vol. 386. pp. 77–104. 1999.

Bechtel SAIC Company, LLC. "Saturated Zone Flow and Transport Model Abstraction." MDL–NBS–HS–000021. Rev. 02. Las Vegas, Nevada: Bechtel SAIC Company, LLC. 2004.

Bellin, A., A. Rinaldo, W.J.P. Bosma, S.E.A.T.M. van der Zee, and Y. Rubin. "Linear Equilibrium Adsorbing Solute Transport in Physically and Chemically Heterogeneous Porous Formations, 1, Analytical Solutions." *Water Resources Research*. Vol. 29, No. 12. pp. 4,019–4,030. 1993.

Berkowitz, B., A. Cortis, M. Dentz, and H. Scher. "Modeling Non-Fickian Transport in Geological Formations as a Continuous Time Random Walk." *Reviews of Geophysics*. Vol. 44, No. RG2003. doi:10.1029/2005RG000178. 2006.

Berkowitz, B., J. Klafter, R. Metzler, and H. Scher. "Physical Pictures of Transport in Heterogeneous Media: Advection-Dispersion, Randomwalk and Fractional Derivative Formulations." *Water Resources Research*. Vol. 38. pp. 1,191. doi:10.1029/2001WR001030. 2002.

Bertetti, F.P., J. Prikryl, and B. Werling. "Development of Updated Total-System Performance Assessment Parameter Distributions for Radionuclide Transport in the Saturated Zone." San Antonio, Texas: CNWRA. 2004.

Bertetti, F.P., R.T. Pabalan, and M.G. Almendarez. "Studies of Neptunium(V) Sorption on Quartz, Clinoptilolite, Montmorillonite, and α-Alumina." *Adsorption of Metals by Geomedia*. E.A. Jenne, ed. New York City, New York: Academic Press, Inc. pp. 131–148. 1998.

Bosma, W.J.P., A. Bellin, S.E.A.T.M. van der Zee, and A. Rinaldo. "Linear Equilibrium Adsorbing Solute Transport in Physically and Chemically Heterogeneous Porous Formations, 2, Numerical Results." *Water Resources Research*. Vol. 29, No. 12. pp. 4,031–4,043. 1993.

Brusseau, M.L. "Transport of Reactive Contaminants in Heterogeneous Porous Media." *Reviews of Geophysics*. Vol. 32, No. 3. pp. 285–313. 1994.

Carle, S.F., M. Zavarin, and G.A. Pawloski. "Geostatistical Analysis of Spatial Variability of Mineral Abundance and K_d in Frenchman Flat, NTS, Alluvium." UCRL–ID–150200. Livermore, California: Lawrence Livermore National Laboratory. 2002.

Cirpka, O.A. "Choice of Dispersion Coefficients in Reactive Transport Calculations on Smoothed Fields." *Journal of Contaminant Hydrology*. Vol. 58. pp. 261–282. 2002.

Cortis, A., C. Gallo, H. Scher, and B. Berkowitz. "Numerical Simulation of Non-Fickian Transport in Geological Formations with Multiple-Scale Heterogeneities." *Water Resources Research*. Vol. 40, No. W04209. doi:10.1029/2003WR002750. 2004.

Cvetkovic, V. and G. Dagan. "Transport of Kinetically Sorbing Solutes by Steady Random Velocity in Heterogeneous Porous Media." *Journal of Fluid Mechanics*. Vol. 265. pp. 189–215. 1994.

Dagan, G. *Flow and Transport in Porous Formations*. New York City, New York: Springer-Verlag. 1989.

Dai, Z., R.W. Ritzi, Jr., C. Huang, Y. Rubin, and D.F. Dominic. "Transport in Heterogeneous Sediments with Multimodal Conductivity and Hierarchical Organization Across Scales." *Journal of Hydrology*. Vol. 294, No. 1–3. pp. 68–86. 2004.

Davis, J.A. NUREG/CR–6708, "Surface Complexation Modeling of Uranium(VI) Adsorption on Natural Mineral Assemblages." Washington, DC: NRC. March, 2001.

de Marsily, G., F. Delay, J. Gonçalvès, P. Renard, V. Teles, and S. Violette. "Dealing With Spatial Heterogeneity." *Journal of Hydrogeology*. Vol. 13. pp. 161–183. 2005.

Durflosky, L.J. "Upscaling and Gridding of Fine Scale Geological Models for Flow Simulation." Proceedings of the 8th International Forum on Reservoir Simulation. June 20–24, 2005, Stresa, Italy*:* 2005.

Farmer, C.L. "Upscaling: A Review." *International Journal for Numerical Methods in Fluids,* Vol. 40. pp. 63–78. 2002.

Farrell, D.A., V. Rankin, and A. Buseman-Williams. "Development and Application of a Model to Simulate Saturated Zone Transport From the Location of the Proposed Repository Footprint at Yucca Mountain." San Antonio, Texas: CNWRA. 2005.

Fernàndez-Garcia, D. and J.J. Gómez-Hernández. "Impact of Upscaling on Solute Transport: Traveltimes, Scale Dependence of Dispersivity, and Propagation of Uncertainty." *Water Resources Research* Vol. 43, No. W02423. doi:10.1029/2005WR004727. 2007.

Gelhar, L.W. "Stochastic Subsurface Hydrology." Old Tappan, New Jersey: Prentice-Hall. 1993.

Gelhar, L.W., C. Welty, and K. Rehfeldt. "A Critical Review of Data on Field-Scale Dispersion Aquifers." *Water Resources Research*. Vol. 28. pp. 1,955–1,974. 1992.

Geomatrix Consultants. "Saturated Zone Flow and Transport Expert Elicitation Project." Deliverable Number SL5X4AM3. Las Vegas, Nevada: CRWMS M&O. 1998.

Ginn, T.R. "Stochastic–convective Transport with Nonlinear Reactions and Mixing: Finite Streamtube Ensemble Formulation for Multicomponent Reaction Systems With Intra-Streamtube Dispersion." *Journal of Contaminant Hydrolology*. Vol. 47, Nos. 1–2. pp. 1–28. 2001.

Haggerty, R. and S.M. Gorelick. "Modeling Mass Transfer Processes in Soil Columns With Pore-Scale Heterogeneity." *Soil Science Society of America Journal*. Vol. 62. pp. 62–74. 1998.

Harvey, C. and S.M. Gorelick. "Rate-Limited Mass Transfer or Macrodispersion: Which Dominates Plume Evolution at the Macrodispersion Experiment (MADE) Site?" *Water Resources Research*. Vol. 36. pp. 637–650. 2000.

Knudby, C. and J. Carrera. "On the Relationship Between Indicators of Geostatistical, Flow and Transport Connectivity." Advances in Water Resources. Vol. 28. pp. 405–421. 2005.

Liedl, R. and T. Ptak. "Modeling of Diffusion-limited Retardation of Contaminants in Hydraulically and Lithologically Nonuniform Media." *Journal of Contaminant Hydrology*. Vol. 66. pp. 239–259. 2003.

Liu, G.S., C.M. Zheng, and S.M. Gorelick. "Limits of Applicability of the Advection-Dispersion Model in Aquifers Containing Connected High-Conductivity Channels." *Water Resources Research*. Vol. 40, No. W08308. doi:10.1029/2003WR002735. 2004.

Lu, Z.M. and D.X. Zhang. "On Stochastic Modeling of Flow in Multimodal Heterogeneous Formations." *Water Resources Research*. Vol. 38, No. 10. pp. 1190. doi:10.1029/2001WR001026. 2002.

Lunt, I.A., J.S. Bridge, and R.S. Tye. "A Quantitative, Three-Dimensional Depositional Model of Qravelly-Braided Rivers." *Sedimentology*. Vol. 51. doi:10.1111/j.1365-3091.2004.00627.x. 2004.

McKenna, S.A., D.D. Walker, and B. Arnold. "Modeling Dispersion in Three-Dimensional Heterogeneous Fractured Media at Yucca Mountain." *Journal of Contaminant Hydrology*., Vols. 62–63. pp. 577–594. 2003.

Naff, R.L., D.F. Haley, and E.A. Sudicky. "High-resolution Monte Carlo Simulation of Flow and Conservative Transport in Heterogeneous Porous Media: 1. Methodology and Flow Results." *Water Resources Research*. Vol. 34. pp. 663– 677. 1998.

NRC. "Risk Insights Baseline Report." Washington, DC: NRC. 2004. http://adamswebsearch.nrc.gov ML040560162 (August 13, 2007).

Nye County Nuclear Waste Repository Project Office. "Early Warning Drilling Program". <http://www.nyecounty.com/ewdpmain.htm>. (February 10, 2007).

Painter, S., V. Cvetkovic, and D. Turner. "Effect of Heterogeneity on Radionuclide Transport in the Alluvium Aquifer Near Yucca Mountain, Nevada." *Ground Water*. Vol. 39, No. 3. pp. 326–338. 2001.

Rehfeldt, K., A.F.P. Tompson, A. Hassan, P. Reimus, and K. Halford. "The Role of Dispersion in Radionuclide Transport—Data and Modeling Requirements." S–N/99205–003. Rev. 01. Las Vegas, Nevada: Stoller-Navarro Joint Venture. 2004.

Ressler, T.R., J.A. Stamatakos, K.D. Ridgeway, and J. Winterle. "Preliminary Hydrostratigraphy of the Valley-Fill Aquifer in Fortymile Wash and the Amargosa Desert." San Antonio, Texas: CNWRA. 2000. <http://adamswebsearch.nrc.gov> ADAMS Accession Number ML020100235. (April 6, 2007).

Rubin, Y. "*Applied Stochastic Hydrogeology*." pp. 416. New York City, New York: Oxford Press. 2003.

Rubin, Y., I.A. Lunt, and J.S. Bridge. "Spatial Variability in River Sediments and its Link With River Channel Geometry." *Water Resources Research*. Vol. 42, No. W06D16. doi:10.1029/2005WR004853. 2006.

Rubin, Y., A.Y. Sun, R. Maxwell, and A. Bellin. "The Concept of Block-Effective Macrodispersivity and a Unified Approach for Grid-Scale- and Plume-Scale-Dependent Transport." *Journal of Fluid Mechanics*. Vol. 395. pp. 161–180. 1999.

Sun, A.Y., R. Ritzi, and D. Sims. "Characterization and Modeling of Alluvium Beneath Fortymile Wash, Nevada." San Antonio, Texas: CNWRA. 2006.

Tompson, A.F.B., C.J. Bruton, and G.A. Pawloski. "Evaluation of the Hydrologic Source Term From the Underground Nuclear Tests in Frenchman Flat and the Nevada Test Site: The CAMBRIC test." UCRL–ID–132300. Livermore, California: Lawrence Livermore National Laboratory. 1999.

Turner, D.R. and R.T. Pabalan. "Abstraction of Mechanistic Sorption Model Results for Performance Assessment Calculations at Yucca Mountain, Nevada." *Waste Management*. Vol. 19. pp. 375–388. 1999.

Wen, X.-H., L.J. Durlofsky, and M.G. Edwards. "Upscaling of Channel Systems in Two Dimensions Using Flow-Based Grids." *Transport in Porous Media*. Vol. 51. pp. 343–366. 2003.

Wen, X.-H. and J.J. Gómez-Hernández. "Numerical Modeling of Macrodispersion in Heterogeneous Media: A Comparison of Multi-Gaussian and Non-Multi-Gaussian Models." *Journal of Contaminant Hydrology*. Vol. 30. pp. 129–156. 1998.

Winterle, J.R. "Evaluation of Alternative Concepts for Saturated Zone Flow: Effects of Recharge and Water Table Rise on Flow Paths and Travel Times at Yucca Mountain." San Antonio, Texas: CNWRA. 2003.

Yates, D.E. "The Structure of the Oxide/Aqueous Electrolyte Interface." Ph.D. thesis, University of Melbourne, Australia. pp. 272. 1975.

Zavarin, M., S.F. Carle, and R.M. Maxwell. "Upscaling Radionuclide Retardation—Linking the Surface Complexation and Ion Exchange Mechanistic Approach to a Linear K_d Approach." UCRL–TR–204713. Livermore, California: Lawrence Livermore National Laboratory. 2004.

APPENDIX A
Particle Tracking Using SLIM-FAST

SLIM-FAST (Maxwell and Tompson, 2006) is a particle-tracking code designed to simulate the migration of dissolved, neutrally buoyant, reactive chemical species in saturated groundwater systems. It is based on explicit Lagrangian Random Walk Particle Tracking (RWPT),[1] where the movement of a large number of numerical particles are traced simultaneously to simulate the concentration and spatial distribution of chemical mass as a function of time.

Compared to the Eulerian methods for solving the advection dispersion equation, the RWPT possesses the following advantages:

- It is free of numerical dispersion and artificial oscillations, which are commonly encountered when using the Eulerian methods to solve advection-dominated problems.
- The computational time for solving fine-scale models with a large number of cells and strong heterogeneities is significantly shorter than the traditional Eulerian, mixed Eulerian-Lagrangian, or total variation diminishing schemes (Salamon, et al., 2006).
- The global mass is automatically conserved.

The movement of particles in a velocity field is driven by a drift term and a Brownian motion term (Salamon, et al., 2006)

$$\mathbf{X}_p(t+\Delta t) = \mathbf{X}_p(t) + \mathbf{A}(\mathbf{X}_p, t)\Delta t + \mathbf{B}(\mathbf{X}_p, t)\cdot\mathbf{Z}(t)\sqrt{\Delta t} \qquad \text{(A–1)}$$

where

Δt is time step, $\mathbf{X}_p(t)$ is particle position at time t, **A** is a drift term, **B** is a displacement matrix, and **Z** is a vector of independent, normally distributed random numbers with zero mean and unit variance. The drift and Brownian motion terms are used to account for the particle advection and dispersion processes in a porous medium and are given as (Maxwell and Tompson, 2006, Eqn B–3).

$$\mathbf{A}(\mathbf{X}_p, t) = \frac{1}{R}\left[\mathbf{u} + \nabla\cdot\mathbf{D} + \mathbf{D}\cdot\nabla(\ln\phi)\right] \qquad \text{(A–2)}$$

$$\mathbf{B}\mathbf{B}^T = 2\mathbf{D}/R \qquad \text{(A–3)}$$

where R is retardation factor, **u** is velocity vector, **D** is pore-scale dispersion tensor, and ϕ is porosity. The last two items on the right-hand-side of (A–2) account for nonuniform distributions of ϕ and **D**.

[1]Lagrangian Random Walk Particle Tracking is used throughout this appendix; consequently, the acronym RWPT will be used.

SLIM-FAST uses a semianalytical solution described in Shafer-Perini and Wilson (1991) to solve for particle velocity streamlines in each grid block, based on linear interpolation of boundary fluxes. Bilinear interpolation is used to calculate the dispersive terms (i.e., $\nabla \cdot \mathbf{D}$ and $\mathbf{B}$) so that the local mass balance is conserved (LaBolle, et al., 1996). The use of the analytical solution in SLIM-FAST makes calculation of the large number of particles (50,000 to 100,000) practical.

As part of the validation process, SLIM-FAST was used to calculate the statistics of solute transport in a two-dimensional, statistically stationary and isotropic porous medium, where a pulse-type line source is assumed and there is no pore-scale dispersion. The first- and second-order moments of the particle displacements are given by Dagan (1989)

$$\mathbf{X}_1 = \mathbf{U}t + \mathbf{X}_0 \tag{A–4}$$

$$X_{11} = \sigma_Y^2 \left\{ 2\tau - 2\left[\frac{8}{3} - \frac{4}{\tau} + \frac{8}{\tau^3} - \frac{8}{\tau^2}\left(1 + \frac{1}{\tau}\right)e^{-\tau} \right] \right\} \tag{A–5}$$

where $\mathbf{U}$ is mean velocity vector, $\mathbf{X}_0$ is the start position of the plume, σ_Y^2 is the variance of ln$K$ (denoted by Y), τ is dimensionless time, $\mathbf{X}_1$ is the first-order moment of the particle displacements, and X_{11} is the second-order moment.

Figure A–1 shows the problem setup for the two-dimensional case, where constant head boundary conditions are imposed along the x direction and no-flow boundary conditions along the y direction. The domain has dimensions of 300 by 300 m (984.3 by 984.3 ft) and is discretized uniformly into 2 by 2-m [6.6 by 6.6-ft] numerical blocks. The mean, variance, and the integral scale of the random ln$K$ field are $\mu_Y = 1.0$, $\sigma_Y^2 = 0.1$, $I_Y = 10$ m [32.8 ft]. Fifty realizations of the ln$K$ fields were generated using the sequential Gaussian simulator module in GSLIB 2.0 (Deutsch and Journel, 1998). The location of the line source is shown in Figure A–1. Note that the initial source was placed four integral scales away from the boundaries to avoid boundary effects (Rubin and Dagan, 1988). For each realization, MODFLOW-2000 was used to solve for the velocity field, and SLIM-FAST was used to perform particle tracking for which 100,000 particles were used to represent the plume.

The particle displacement statistics were calculated based on the ensemble statistics from the 50 realizations, using the approach described in Rubin (2003, p. 240). Figure A–2 compares the analytical solution with the SLIM-FAST solution, where a close match between the two is found.

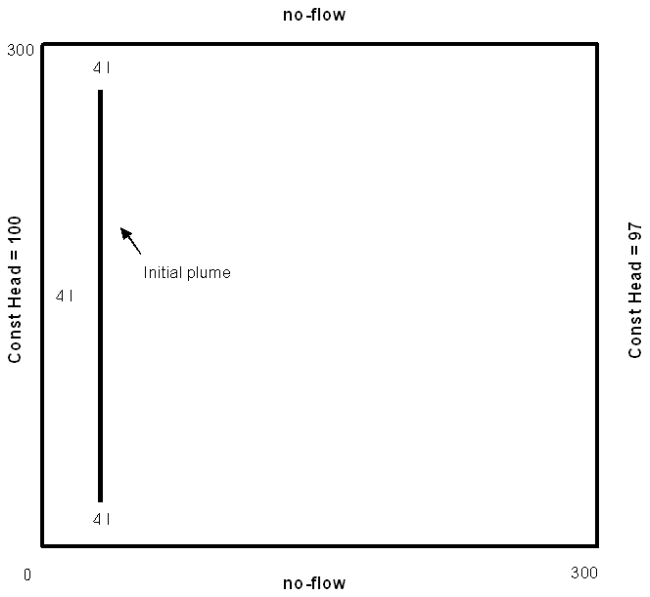

Figure A–1. Problem Configuration for the Two-Dimensional Validation Problem. The Line Source Is Located Four Integral Scales From the Boundaries.

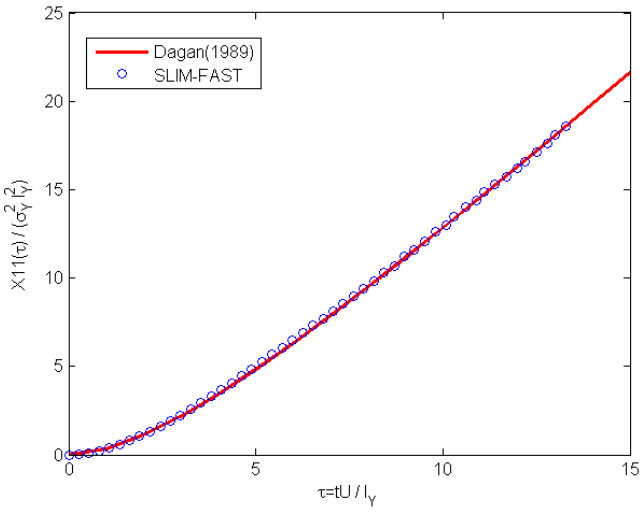

Figure A–2. Comparison Between the Particle Displacement Autocovariance (X_{11}) Obtained by Using SLIM-FAST and the Analytical Solution of Dagan (1989). A Close Match Is Achieved. τ is Dimensionless Travel Time, σ_Y and I_Y Are the Variance and Integral Scale of ln*K*, Respectively.

The total mass was monitored so that the particle tracking was stopped whenever the first particle crossed the right boundary.

References

Dagan, G. Flow and Transport in Porous Formations. New York City, New York: Springer-Verlag. 1989.

Deutsch, C.V. and A.G. Journel. "Geostatistical Software Library and Users Guide." Second Edition. New York City, New York: Oxford University Press. 1998.

LaBolle, E.M., G.E. Fogg, and A.F.B. Tompson. "Random-Walk Simulation of Transport in Heterogeneous Porous Media: Local Mass-Conservation Problem and Implementation Methods. *Water Resources Research*. Vol. 32, No. 3 pp. 583–593. 1996.

Maxwell, R.M. and A.F.B. Tompson. "SLIM-FAST: A Users Manual." UCRL–SM–225092. Livermore, California: Lawrence Livermore National Laboratory. 2006.

Rubin, Y. *Applied Stochastic Hydrogeology*. New York City, New York: Oxford Press. 416 pp. 2003.

Rubin, Y. and G. Dagan. "Stochastic Analysis of Boundary Effects on Head Spatial Variability in Heterogeneous Aquifer, 1. Constant Head Boundary." *Water Resources Research*. pp. 1689–1697. 1988.

Salamon, P., D. Fernàndez-Garcia, and J.J. Gómez-Hernández. "A Review and Numerical Assessment of the Random Walk Particle Tracking Method." *Journal of Contaminant Hydrology*. Vol. 87, pp. 277–305. 2006.

Schafer-Perini, A.L. and J.L. Wilson. "Efficient and Accurate Front Tracking for Two-Dimensional Groundwater Flow Models, *Water Resources Research*. Vol. 27 No.7. 1991.

APPENDIX B
Np-237 Sorption Data (K_A) Used in This Report

Table B–1 Np-237 Sorption Data (K_A) Used in This Report					
No.	**Region**	**Well**	**X (m)***	**Y (m)**	**ln(K_A)**
1	Amargosa Valley	Airport Well	552846.00	4054904.00	1.40
2	Amargosa Valley	15S/50E-18cc	553710.00	4055273.00	1.16
3	Amargosa Valley	NC-EWDP-4PA	553167.00	4056766.00	1.03
4	Amargosa Valley	15S/50E-19b1	553862.50	4054720.00	0.95
5	Amargosa Valley	15S/50E-18cd	553934.30	4055151.00	0.89
6	Amargosa Valley	NDOT	553685.00	4055242.00	0.89
7	Amargosa Valley	Desert Farms	553295.00	4055305.00	0.76
8	CNWRA	NC-EWDP-19IM2	549258.00	4058286.00	1.32
9	CNWRA	NC-EWDP-19IM1	549238.00	4058286.00	1.32
10	CNWRA	NC-EWDP-16P	545586.00	4064259.00	1.22
11	CNWRA	NC-EWDP-19PBs	549250.00	4058288.00	1.15
12	CNWRA	NC-EWDP-29P	549318.00	4059602.00	1.14
13	CNWRA	NC-EWDP-28P	545666.00	4062389.00	1.14
14	CNWRA	NC-EWDP-18P	549337.00	4067229.00	0.96
15	CNWRA	NC-EWDP-27P	544856.00	4065271.00	1.02
16	CNWRA	NC-EWDP-19D	549238.00	4058265.00	0.98
17	CNWRA	NC-EWDP-10Ps	553070.00	4064911.00	0.65
18	CNWRA	NC-EWDP-10S1	553061.00	4064895.00	0.65
19	CNWRA	NC-EWDP-24P	549307.00	4062051.00	0.70
20	CNWRA	NC-EWDP-22PBs	551959.00	4062032.00	0.62
21	CNWRA	NC-EWDP-19P	549250.00	4058287.00	0.54
22	CNWRA	NC-EWDP-22S1	551940.00	4062016.00	0.41
23	CNWRA	NC-EWDP-22PAs	551941.00	4062034.00	0.32
24	CNWRA	NC-EWDP-07SC1	539558.00	4064320.00	0.39
25	Crater Flat	GexaWell4	534069.00	4086110.00	0.82
26	Crater Flat	VH-1	539976.00	4071714.00	0.58

Table B–1. Np-237 Sorption Data (K_A) Used in This Report (Continued)					
No.	**Region**	**Well**	**X (m)***	**Y (m)**	**ln(K_A)**
27	Forty Mile Wash North	JF#3	554498.00	4067974.00	0.68
28	Forty Mile Wash North	UE-29a#1 HTH	555758.00	4088341.00	0.60
29	Forty Mile Wash North	WT#15	554034.00	4078702.00	0.50
30	Forty Mile Wash North	WT#14	552630.00	4077330.00	0.34
31	Forty Mile Wash North	J-13	554017.00	4073517.00	0.26
32	Forty Mile Wash North	J-12	554444.00	4068774.00	0.17
33	Forty Mile Wash North	a#2(sh)	555753.00	4088351.00	0.07
34	Forty Mile Wash East	15S/49E-22a1	550086.30	4054974.00	0.89
35	Forty Mile Wash East	15S/49E-27ac	549552.90	4052722.00	0.74
36	Forty Mile Wash East	15S/49E-22dc	549672.50	4053523.00	−0.29
37	Jackass Flat	UE-25 J-11	563798.00	4071073.00	0.98
38	Solitario Canyon Wash	WT-7	546151.00	4075474.00	1.22
39	Solitario Canyon Wash	WT-10	545964.00	4073378.00	1.12
40	Solitario Canyon Wash	H-6(Tcb)	546188.00	4077816.00	1.03
41	Southern Yucca Mountain	NC-EWDP-3S Z2	541273.00	4059444.00	1.24
42	Southern Yucca Mountain	NC-EWDP-9SX1	539040.00	4061006.00	1.06
43	Southern Yucca Mountain	NC-EWDP-03D	541273.00	4059444.00	1.10
44	Southern Yucca Mountain	NC-EWDP-09SX	539039.00	4061004.00	0.88
45	Southern Yucca Mountain	NC-EWDP-15P	544848.00	4058158.00	0.74
46	Southern Yucca Mountain	CIND-R-LITE	544027.00	4059809.00	0.72
47	Southern Yucca Mountain	NC-EWDP-02D	547744.00	4057164.00	0.51
48	South West Crater Flat	NC-EWDP-12PC	536872.00	4060809.00	0.48
49	South West Crater Flat	NC-EWDP-1S Z1	536771.00	4062499.00	0.40
50	South West Crater Flat	NC-EWDP-1S	536771.00	4062499.00	0.31

Table B–1. Np-237 Sorption Data (K_A) Used in This Report (Continued)					
No.	**Region**	**Well**	**X (m)***	**Y (m)**	**ln(K_A)**
51	South West Crater Flat	NC-EWDP-7S	539558.00	4064318.00	0.31
52	South West Crater Flat	NC-EWDP-1DX	536768.00	4062503.00	0.21
53	South West Crater Flat	VH-2	537738.00	4073214.00	0.10
54	South West Crater Flat	NC-EWDP-12PB	536873.00	4060794.00	-0.09
55	South West Crater Flat	NC-EWDP-12PA	536906.00	4060766.00	-0.20
56	Yucca Mountain Central	UZ#16	549484.90	4076986.00	1.41
57	Yucca Mountain Central	G-4	548933.00	4078602.00	0.67
58	Yucca Mountain Central	H-4	549188.00	4077309.00	0.41
59	Yucca Mountain Central	b#1(Tcb)	549949.00	4078423.00	0.15
60	Yucca Mountain Crest	H-3	547562.00	4075759.00	1.26
61	Yucca Mountain Crest	UZ-14(sh)	548032.00	4080260.00	1.17
62	Yucca Mountain Crest	USW SD-6	547592.00	4077514.00	1.12
63	Yucca Mountain Crest	USW WT-24	548691.00	4081898.00	0.83
64	Yucca Mountain Crest	H-5	547668.00	4078841.00	0.82
65	Yucca Mountain Crest	H-1(Tcb)	548727.00	4079926.00	0.67
66	Yucca Mountain Crest	G-2	548143.00	4082542.00	0.51
67	Yucca Mountain South West	ONC#1	550479.90	4076608.00	1.40
68	Yucca Mountain South West	c#3	550930.00	4075902.00	0.66
69	Yucca Mountain South West	c#2	550955.00	4075871.00	0.66
70	Yucca Mountain South West	WT#3	552090.00	4072550.00	0.59
71	Yucca Mountain South West	WT#12	550168.00	4070659.00	0.58
72	Yucca Mountain South West	c#1	550955.00	4075933.00	0.58

Table B–1. Np-237 Sorption Data (K_A) Used in This Report (Continued)					
No.	**Region**	**Well**	**X (m)***	**Y (m)**	**ln(K_A)**
73	Yucca Mountain South West	WT-17	549905.00	4073307.00	0.16
74	Yucca Mountain South West	p#1(v)	551501.00	4075659.00	-0.20
*Coordinates are measured in UTM. 1 m = 3.28 ft					